Cooperative effects in photon statistics of molecular dimers with spectral diffusion

František Šanda and Shaul Mukamel[a)]
Department of Chemistry, University of California, Irvine, California 92697-2025

(Received 26 October 2005; accepted 18 January 2006; published online 23 March 2006)

The two-point fluorescence intensity correlation function $g^{(2)}(t)$ and the Mandel parameter $M(t)$ are calculated for a strongly pumped dimer of two-level molecules undergoing Gaussian-Markovian frequency fluctuations. The effects of detuning and saturation are examined. All fluctuation time scale regimes are explored using a continued fraction solution of the stochastic Liouville equation for the generating function. Bunching and antibunching are observed for slow and fast fluctuations, respectively. The short-time antibunching dip in $g^{(2)}$ and its variation with intermolecular coupling, the exciton annihilation rate, and laser detuning are studied. © *2006 American Institute of Physics*. [DOI: 10.1063/1.2174001]

I. INTRODUCTION

The optical properties of coupled molecules in organic crystals,[1–3] photosynthetic antennae[4–6] and *J* aggregates[7] have drawn considerable attention. Quantum entanglement of chromophores in complexes with well defined orientation of transition dipoles gives rise to collective super- and subradiance emission and absorption.[8] Depending on the magnitude and time scale of fluctuations, coupled chromophores may either be independent or behave as a single supermolecule.[9] A large aggregate may be divided into a number of regions, each behaving as a single emitter. The correlation length associated with the collective spontaneous emission (superradiance) rate provides a direct measure of cooperativity, and the interplay of intermolecular coupling, static disorder, temperature, and polaron formation has been investigated.[10–14]

Single molecule spectroscopy (SMS) provides a new tool for studying environment fluctuations in the condensed phase.[15–20] Unlike bulk measurements, SMS can distinguish between static disorder and dynamical fluctuations, and directly measures the entire inhomogenous distributions of system parameters such as fluorescence rates.[21,22] Recent advances in single molecule spectroscopy were reviewed by Kulzer and Orrit.[23] The main effort has focused on analyzing the autocorrelation function $g^{(2)}$ and the factorial moments of photon counting statistics, the distributions of on/off blinking times,[24] time-dependent lineshapes,[25,26] and consecutive photon statistics.[27,28]

A single two-level system (TLS) is unable to emit two photons in a short time interval.[29–31] The resulting dark period after emission known as *photon antibunching* is suppressed when several independent emitters contribute to the fluorescence.[32] The probability of two simultaneous photon emissions has thus been suggested as a measure of the number of independently emitting regions in the aggregate.[33–38] One complication with this measure is exciton-exciton annihilation[39,40] which can produce similar antibunching.

Photon statistics in interacting chromophores has been studied since 1970s. A homodimer has a symmetric (superradiant) and an antisymmetric (subradiant) one-exciton states and the quantum jumps between them result in on and off periods (blinking),[41,42] similar to that reported in single molecule triplet state dynamics.[43–45] Blinking is connected with photon bunching.[46] Fluorescence statistics from perylenmonoimide chromophores coupled via a benzyl motif (benzilic biperilenemonoimide) showed blinking and mild bunching on the ~0.1 ms scale. This blinking is attributed to switching to a dark triplet state and allows the determination of its rate. Antibunching reported on the nanosecond scale is incompatible with the independent chromophores picture and was attributed to exciton-exciton annihilation.[34] Slow transitions (jumps) between the localized and delocalized regimes of individual biperylenimide molecules were associated with changes in fluorescence intensities. The distributions of radiative rates were measured.[21]

Two-photon absorption is another signature of coupling in dimers.[47] Subsequent two photon emission can show both bunching and antibunching depending on the system parameters.[48] Two-photon resonances were found in the fluorescence of terrylene dimers in a *p*-terphenyl matrix, and the exciton parameters were determined by fitting to the Bloch equations.[49]

Measurements of the fluorescence intensity correlation function $g^{(2)}$ were conducted on larger aggregates, biological antenna complexes, and dendrimers.[35–38] Experiments on B-phycoerythrin (with 34 chromophores) showed that individual molecules can emit one photon at a time.[36] In contrast, the four chromophores of tetrahedraoligophenylenvinylene were found to emit consistently with the three-emitter pictures.[35] Conformational effects in single chain photon emission from the conjugated polymer poly[2-methoxy,5-(2-ethyl-hexyloxy)-p-phenylene-vinylene] (MEH-PPV) were demonstrated—polymers in the collapsed-chain conformation but not in the extended-chain structures, which showed photon antibunching.[37] Low temperature study of light-

[a)]Electronic mail: smukamel@uci.edu

harvesting 11o complex of *Rhodopseudomonas acidophila* yielded the distribution of the first moment of the lineshape as well as the coupling strength.[50,51] Two types of fluorescence fluctuation behavior were observed in three-chromophoric dendrimeric molecules; different isomers may or may not show triplet state on-off blinking, depending on the singlet/triplet energy gap.[52]

This experimental effort has been accompanied by extensive theoretical modeling. Early analysis of SMS signals in nonfluctuating resonant TLS showed antibunching.[29,30] Spontaneous or photoinduced spectral fluctuations caused by changes in the environment are significant.[53] These may appear on arbitrary time scales;[54] fast fluctuations can be accounted for by simply adding dephasing rates,[55] whereas slow fluctuations lead to time intervals whereby the TLS absorbs and emits effectively (bunching). When the relaxation time scales of electronic (fast) and bath (slow) degrees of freedom are well separated, the fast component may be obtained by static averaging over electronic relaxation, and the slow component is obtained by assuming instantaneous relaxation of the electronic degrees of freedom and only considering the environment dynamics.[56,57]

The Kubo-Anderson two-state-sudden-jump model of spectral diffusion[58,59] is the simplest stochastic Markovian model of environment fluctuations[60] in lineshapes of low temperature glasses.[61–64] The mean fluorescence yield and the second factorial moment were used to calculate the Mandel parameter M for this model using a semiclassical approximation and a perturbative solution of stochastic Liouville equations in the driving field. The second factorial moment was expressed in terms of four-point dipole correlation functions[65,66] similar to nonlinear four wave mixing spectroscopy.[67]

Zheng and Brown[68] recently went beyond the semiclassical approximation and employed the generating function formalism[60,69–73] to calculate M for the Kubo-Anderson model. In the long-time limit M was expressed in a closed form.[74] Fast Gaussian-Markovian fluctuations were considered as well.[68] Very slow fluctuations were described by assuming time scale separation between electronic and bath dynamics.[57] The quantum jump (Monte Carlo wave function) approach[75,76] is an alternative to the generating function approach.

In this paper we calculate $g^{(2)}$ and M for the Gaussian-Markovian model of spectral diffusion (Ornstein-Uhlenbeck process)[77] in a dimer of two-level molecules. Frequency fluctuations are caused by coupling the molecules to Brownian oscillator modes. The entire parameter space is explored using a continued fraction solution[78–80] of the generating function. The effects of slow and fast fluctuations, detuning, and saturation are studied. The Bloch equation model[49] is recovered for fast fluctuations. The short-time dip in $g^{(2)}$ is studied. Weak field linear absorption lineshape can be described in terms of the single exciton manifold. $g^{(2)}$, in contrast, depends on the two-exciton manifold and directly probes the effects of two-photon absorption, emission, and exciton annihilation. We compare antibunching caused by exciton annihilation and intermolecular coupling and study its variation with the fluctuation time scale and detuning.

The stochastic model of spectral diffusion is introduced in Sec. II, and the generating function formalism is used in Sec. III to calculate $g^{(2)}$ and M. The fast fluctuation limit is discussed in Sec. IV. Arbitrary fluctuation time scales are simulated for a monomer in Sec. V and for a dimer in Sec. VI. Our results are summarized in Sec. VII.

II. SPECTRAL DIFFUSION IN AGGREGATES

We describe a molecular aggregate made of coupled TLS using the Frenkel exciton Hamiltonian:[10,22,81,82]

$$H_0 = \sum_n \epsilon_n \hat{B}_n^\dagger \hat{B}_n + \sum_{mn} J_{mn} \hat{B}_m^\dagger \hat{B}_n, \tag{1}$$

where ϵ_n is the energy of nth chromophore, and J_{mn} are the hopping integrals. In this paper we set $\hbar = 1$. $\hat{B}_n$ ($\hat{B}_n^\dagger$) are the annihilation (creation) operators satisfying the Pauli commutation relations,

$$[\hat{B}_n, \hat{B}_m^\dagger] = \delta_{m,n}(1 - 2\hat{B}_m^\dagger \hat{B}_n),$$

which imply that each molecule can carry at most a single excitation. The complete basis set consists of the ground state $|g\rangle$, the one-exciton manifold $|n\rangle \equiv \hat{B}_n^\dagger |g\rangle$, the two-exciton manifold $|nm\rangle \equiv \hat{B}_n^\dagger \hat{B}_m^\dagger |g\rangle$, and higher excitonic manifolds $|n \cdots m\rangle \equiv \hat{B}_n^\dagger \cdots \hat{B}_m^\dagger |g\rangle$. We shall denote this basis by indices i, j, k, and l.

Each molecule has a dipole moment $\boldsymbol{\mu}_n$. Its interaction with the optical electric field $\mathbf{E}$ with frequency ω is represented in the interaction representation defined by the unitary transformation,

$$\rho(t) = \exp(i\mathcal{H}t)\tilde{\rho}(t)\exp(-i\mathcal{H}t), \tag{2}$$

where $\mathcal{H} \equiv \omega \Sigma_n \hat{B}_n^\dagger \hat{B}_n$ is the generator of this tranformation, and ρ ($\tilde{\rho}$) is the aggregate density matrix in the interaction (Schrödinger) picture. The transformation [Eq. (2)] commutes with projectors onto the various exciton manifolds; it does not affect H_0 and the dynamics of population and coherences within each manifold. For coherences between different manifolds ρ_{ij}, it adds a factor $\omega_{ij} \equiv \langle i|\mathcal{H}|i\rangle - \langle j|\mathcal{H}|j\rangle$ to the equation of motion,

$$\frac{d\rho(t)}{dt} = i[\mathcal{H}, \rho] + \exp(i\mathcal{H}t)\frac{d\tilde{\rho}(t)}{dt}\exp(-i\mathcal{H}t), \tag{3}$$

where $[\mathcal{H}, \rho]_{ij} = \omega_{ij}\rho_{ij}$.

Assuming that the dipole moments are paralel $\boldsymbol{\mu}_n = \boldsymbol{\mu}$, we define $\mu^+ = \Sigma_n B_n^\dagger$ and $\mu^- = \Sigma_n B_n$, and the Rabi frequency is given by $\mathcal{E} \equiv (\mathbf{E} \cdot \boldsymbol{\mu})$. In the interaction picture [Eq. (2)] the Hamiltonian assumes the time independent form in the rotating wave approximation:

$$H_S = H_0 - \mu^+(\mathcal{E}/2) - \mu^-(\mathcal{E}/2). \tag{4}$$

The time evolution of the driven system, including spontaneous emission, is described by the master equation for the density matrix ρ in the interaction picture:[83,84]

$$\frac{d\rho_{ij}(t)}{dt} = i\omega_{ij}\rho_{ij} + \sum_{kl} (i(H_S)_{lj}\delta_{ik} - i(H_S)_{ik}\delta_{jl} + \mathcal{K}_{ijkl} + \gamma_{ijkl})\rho_{kl}(t) \equiv \mathcal{L}_S\rho(t). \quad (5)$$

Here

$$\mathcal{K}_{ijkl} = \Gamma\langle i|\mu^-|k\rangle\langle l|\mu^+|j\rangle - \Gamma/2(\delta_{ik}\langle l|\mu^+\mu^-|j\rangle + \delta_{jl}\langle i|\mu^+\mu^-|k\rangle) \quad (6)$$

are the radiative decay rates, where Γ is the radiative decay rate of the monomer. Equation (6) assumes aggregates with parallel dipole moments located within area, small compared to the wavelength of the emitted light, so that electric field acts on all molecules with the same phase (Dicke superradiance[8]).

γ represents exciton-exciton annihilation, which is modeled as a transition from the two-exciton manifolds to the one-exciton manifold with rates[85] $\gamma_{mn,m'n',mn,m'n'} = -\gamma(\delta_{n,m\pm1} + \delta_{m',n'\pm1})$; $\gamma_{m,m,mn,mn} = \gamma\delta_{n,m\pm1}$; $\gamma_{mn,m',mn,m'} = \gamma_{m',mn,m',mn} = -\gamma\delta_{m,n\pm1}$; $\gamma_{mn,g,mn,g} = \gamma_{g,mn,g,mn} = -\gamma\delta_{m,n\pm1}$. This assumes that the double excitation at two neighboring sites is damped and decays with the same rate γ to one of the molecules.

The system is further coupled to uncorrelated Brownian oscillator bath coordinates Q_u which induce site energy fluctuations,

$$H_{\mathrm{SB}} = \sum_{un} T_{un}Q_u(t)\hat{B}_n^\dagger\hat{B}_n. \quad (7)$$

In Liouville space the system-bath interaction is described by the superoperator $\mathcal{L}_{\mathrm{SB}} \equiv -i[H_{\mathrm{SB}}, \ldots]$,

$$\mathcal{L}_{\mathrm{SB}} = \sum_u Q_u D_u, \quad (8)$$

where D_u operates on the system subspace

$$D_u\rho = -i\sum_n T_{un}[\hat{B}_n^\dagger\hat{B}_n, \rho].$$

The evolution of Q_u in the high temperautre limit is described by the Fokker-Planck operator,

$$\mathcal{L}_B = \sum_u \Lambda_u \frac{\partial}{\partial Q_u}\left(Q_u + \sigma_u^2\frac{\partial}{\partial Q_u}\right). \quad (9)$$

Λ_u is the inverse autocorrelation time, and σ_u is the variance of the equilibrium distribution.

Altogether, our model is given by the stochastic Liouville equation:

$$\frac{\partial}{\partial t}\rho = \mathcal{L}\rho(t), \quad (10)$$

with

$$\mathcal{L} = \mathcal{L}_S + \mathcal{L}_B + \mathcal{L}_{\mathrm{SB}}. \quad (11)$$

$\mathcal{L}_S$ [Eq. (5)] describes the system, $\mathcal{L}_B$ [Eq. (9)] represents the bath, and $\mathcal{L}_{\mathrm{SB}}$ [Eq. (8)] is their interaction. The driven system is initially assumed to be in steady state so that $\mathcal{L}\rho(0)=0$. Since in the interaction picture [Eq. (2)], $\mathcal{L}$ is time independent, Eq. (10) may be solved by algebraic methods. We shall expand the bath variables in the basis of eigenvectors of Fokker-Planck operator (see Appendix A).

III. THE GENERATING FUNCTION FOR SINGLE-PHOTON COUNTING

In a photon counting experiment individual photons are observed. For a given time window t the number $n(t)$ of emitted photons is recorded and its statistical properties are analyzed. The time resolved fluorescence intensity I is given by

$$I(t) \equiv \frac{n(t+\Delta t) - n(t)}{\Delta t}, \quad \Delta t \to 0. \quad (12)$$

We shall calculate the two common SMS observables. The first is the autocorrelation function $g^{(2)}$ of the fluorescence intensity:

$$g^{(2)}(\tau) \equiv \frac{\langle I(t+\tau)I(t)\rangle}{\langle I(t+\tau)\rangle\langle I(t)\rangle}. \quad (13)$$

At steady state $g^{(2)}$ only depends on τ and is independent on t. The stochastic nature of photon counting experiments stems from the bath-induced fluctuations of site energies and the unpredictability of individual spontaneous photon emissions which is essentialy a quantum phenomenon. $\langle\ \rangle$ denotes averaging over both these sources of stochasticity.

The statistical distribution of recorded photons may be characterized by its moments. The Mandel parameter is defined by the following combination of the first two moments:[86]

$$M(t) \equiv \frac{\langle(n(t) - \langle n(t)\rangle)^2\rangle - \langle n(t)\rangle}{\langle n(t)\rangle}, \quad (14)$$

where $M=0$ ($M<0$) indicates Poissonian (sub-Poissonian) statistics.

We next turn to the resetting superoperator[87] R which connects the density matrix right before (ρ) and after (ρ') the observation of a photon, $\rho' = R\rho$. A monomer is necessarily in the ground state after emission. For aggregates we follow the resetting procedure suggested in Ref. 87 which depends on the positive rates in the master equation [Eq. (5)],

$$R_{ijkl} = \Gamma\langle i|\mu^-|k\rangle\langle l|\mu^+|j\rangle. \quad (15)$$

Equation (15) assumes that the photons are not resolved spectrally. Generally it is not possible to tell from which site (or level) a photon was emitted, and the resetting superoperator [Eq. (15)] may not be decomposed into a sum of terms attributed to a transition from a particular site (levels). Let us consider the emission from the one-exciton manifold of a dimer whose site energies differ by $\delta\epsilon$. Neglecting Γ and J the density matrix evolves as

$$\rho = \tfrac{1}{2}(|1\rangle\langle 1| + e^{i\delta\epsilon t}|1\rangle\langle 2| + e^{-i\delta\epsilon t}|2\rangle\langle 1| + |2\rangle\langle 2|),$$

and the fluorescence oscillates as $\Gamma\Sigma_{ij=1}^2\rho_{ij} = \Gamma(1+\cos\,\delta\epsilon t)$. For large $\delta\epsilon$ the oscillations are too fast to be resolved and can be averaged so that R_{gg12}, R_{gg21} contributions (and similar terms in the master equation) can vanish. This corre-

sponds to the secular approximation in the Redfield theory.[88] Setting $R_{gg12},R_{gg21}=0$, cooperativity is lost and frequency resolved detection from different sites is described by the matrices $R^{(n)}(=R_{ggnn}|gg\rangle\langle nn|)$, which satisfy $R=\Sigma_n R^{(n)}$.

Generating functions provide a convenient tool for calculating factorial moments of photon statistics.[50,68–73,89] We first define a generating functional by the differential equation,

$$\frac{d\mathcal{G}(t;s)}{dt}=\mathcal{L}\mathcal{G}(t;s)-(1-s)R\mathcal{G}(t;s), \tag{16}$$

with boundary condition $\mathcal{G}(0;s)=1$. s is a real parameter; for $s=1$ $\mathcal{G}$ coincides with the ordinary evolution superoperator $\mathcal{U}(t)\equiv\mathcal{G}(t;1)$.

The generating function is obtained by averaging the functional over initial states and summing over the final states,

$$\bar{\mathcal{G}}(t;s)\equiv\langle\langle \mathrm{Tr}\mathcal{G}(t;s)\rho(0)\rangle\rangle, \tag{17}$$

where the trace is over system variables, and $\langle\langle\ \rangle\rangle$ denotes averaging over bath variables. The factorial moments may be calculated by differentiation with respect to s:

$$\langle n(n-1)\ldots(n-m+1)\rangle=\frac{\partial^m}{\partial s^m}\bar{\mathcal{G}}(t;s)\bigg|_{s=1} \tag{18}$$

This gives, for M [Eq. (14)],

$$M(t)=\frac{(\partial^2/\partial s^2)\bar{\mathcal{G}}(t;s)|_{s=1}}{(\partial/\partial s)\bar{\mathcal{G}}(t;s)|_{s=1}}-\frac{\partial}{\partial s}\bar{\mathcal{G}}\,(t;s)|_{s=1}. \tag{19}$$

The autocorrelation function [Eq. (13)] is given by

$$g^{(2)}(t)=\frac{\langle\langle \mathrm{Tr}R\mathcal{U}(t)R\rho(0)\rangle\rangle}{\langle I\rangle^2}, \tag{20}$$

where the steady state emission,

$$\langle I\rangle=\langle\langle \mathrm{Tr}R\rho(0)\rangle\rangle, \tag{21}$$

has a close connection to absorption lineshape I_A, which is obtained by accounting for the annihilated excitations,

$$I_A(\omega)=\langle I\rangle+2\gamma\sum_n \rho_{nn+1,nn+1}. \tag{22}$$

Introducing the Laplace transform $\tilde{\mathcal{G}}(z;s)\equiv\int_0^\infty e^{-z\tau}\mathcal{G}(\tau;s)d\tau$, the formal solution of Eq. (16) is

$$\tilde{\mathcal{G}}(z;s)=\frac{1}{z-\mathcal{L}+(1-s)R}. \tag{23}$$

$\tilde{\mathcal{G}}$ is a matrix in the joint system-bath space. Using the matrix representation of the linear coupling [Eq. (A3)], the matrix in the denominator of Eq. (23) is tridiagonal in the bath space and its inverse can be recast in a continued fraction form.[78,79] Its most relevant element for the current applications is

$$\tilde{\mathcal{G}}_{0,0}(z;s)=\left[\mathcal{X}-\begin{pmatrix}\sigma_1 D_1\\ \sigma_2 D_2\\ \cdots\end{pmatrix}^T\left[\begin{pmatrix}\mathcal{X}+\Lambda_1 & 0 & 0\\ 0 & \mathcal{X}+\Lambda_2 & \cdots\\ \cdots & \cdots & \cdots\end{pmatrix}+\cdots\right]^{-1}\times\begin{pmatrix}\sigma_1 D_1\\ \sigma_2 D_2\\ \cdots\end{pmatrix}\right]^{-1}, \tag{24}$$

where we have denoted $\mathcal{X}\equiv z-\mathcal{L}_S+(1-s)R$.

The derivatives with respect to s were obtained analytically in Appendix C.

$$\frac{\partial}{\partial s}\tilde{\bar{\mathcal{G}}}(z;s)\bigg|_{s=1}=\frac{1}{z^2}\langle\langle \mathrm{Tr}R\rho(0)\rangle\rangle,$$
$$\frac{\partial^2}{\partial s^2}\tilde{\bar{\mathcal{G}}}(z;s)\bigg|_{s=1}=\frac{2}{z^2}\langle\langle \mathrm{Tr}R\tilde{\mathcal{U}}(z)R\rho(0)\rangle\rangle. \tag{25}$$

In our simulations we found Eq. (25) to be numerically favorable compared to finite differentiation.

Note that the generating superoperator [Eq. (23)] can be defined for an arbitrary initial density matrix, while Eq. (25) is limited to a steady state [Eq. (C5)]. Equation (17) is more accurate since we only approximate the initial conditions, while Eq. (25) implies that the system starts from an approximate state after each photon emission.

For stationary processes correlation functions and factorial moments carry the same information since $\langle n\rangle=\langle I\rangle t$, and comparison of Eqs. (25) and (20) shows that M and $g^{(2)}$ are simply connected by[30,90]

$$M(t)=\frac{2\langle I\rangle}{t}\int_0^t dt_1\int_0^{t_1}dt_2[g^{(2)}(t_2)-1]. \tag{26}$$

In the long-time limit the distribution of detected photons becomes Gaussian and is characterized solely by the mean number $\langle n\rangle$ and the asymptotic Mandel parameter [see Eqs. (C6) and (C7)]:

$$M(\infty)=\frac{2}{\langle I\rangle}\lim_{\delta\to 0}\mathrm{Re}\langle\langle \mathrm{Tr}R\tilde{\mathcal{U}}(i\delta)R\rho(0)\rangle\rangle. \tag{27}$$

The steady state distribution is calculated as the asymptotic state of the evolution. In Laplace space it is described by the residue of the generating superoperator at $z=0$,

$$\rho_{j\alpha}(0)=\lim_{z\to 0+}z\tilde{\mathcal{U}}_{j\alpha,k\beta}(z). \tag{28}$$

Note that the steady state is independent on initial conditions (i.e., the indices $k\beta$).

IV. THE FAST FLUCTUATION LIMIT

The full width at half maximum of the weak field absorption lineshape can be represented by the Padé approximant,[67]

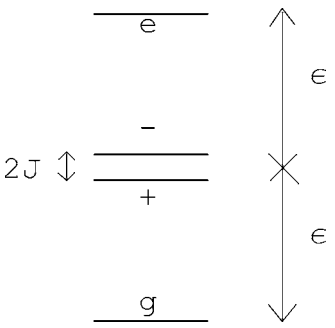

FIG. 1. Exciton level scheme for a dimer.

$$\Gamma_\sigma = \sigma \frac{2.355 + 1.76(\Lambda/\sigma)}{1 + 0.85(\Lambda/\sigma) + 0.88(\Lambda/\sigma)^2}. \tag{29}$$

Holding Γ_σ fixed, the dimensionless parameter $\kappa \equiv (\Lambda/\sigma)$ may be used to distinguish between the slow ($\kappa \ll 1$) and the fast ($\kappa \gg 1$) fluctuation regimes. For fast fluctuations we can truncate the continued fraction Eq. (24) at the first level.

$$\tilde{\mathcal{G}}_{0,0}(z;s) = \frac{1}{z - \mathcal{L}_S + (1-s)R - \Sigma_u D_u(\sigma_u^2/\Lambda_u)D_u}. \tag{30}$$

Fast fluctuations can thus be incorporated by simply adding the dephasing rates σ_u^2/Λ_u to the radiative decay. The total dephasing rate between states i and j will be denoted by $\hat{\Gamma}_{ij}$. For a monomer coupled to a Brownian oscillator we have $\hat{\Gamma}_{eg} = \sigma^2/\Lambda + \Gamma/2$. This limit is described by the Bloch equations and its SMS characteristics have been studied already.[55] The bath is equilibrium at all times. All dynamical information is contained in two-time correlations, and n-time quantities may be factorized as

$$g^{(n)}(\tau_1, \tau_2, \ldots, \tau_{n-1}) = \prod_{i=1}^{n-1} g^{(2)}(\tau_i).$$

$g^{(2)}$ and M for a strong resonantly pumped monomer are given in Eqs. (D3) and (D4). $g^{(2)}$ for a nonresonant weak field is given by Eq. (D6).

We next turn to a dimer. Each site frequency ϵ_n is modulated by an overdamped Brownian oscillator ($T_{un} = \delta_{un}$), and the same parameters, $\sigma_1 = \sigma_2$ and $\Lambda_1 = \Lambda_2$, are assumed. We distinguish between three limits.

(a) *Collective emission* ($J \equiv J_{12} \gg |\epsilon_1 - \epsilon_2|$). We assume identical molecules ($\epsilon_1 = \epsilon_2$) and introduce the following basis set (Fig 1.):

$$|+\rangle = \frac{1}{\sqrt{2}}(\hat{B}_1^\dagger + \hat{B}_2^\dagger)|g\rangle, \quad |-\rangle = \frac{1}{\sqrt{2}}(\hat{B}_1^\dagger - \hat{B}_2^\dagger)|g\rangle,$$
$$|e\rangle = \hat{B}_1^\dagger \hat{B}_2^\dagger |g\rangle. \tag{31}$$

Only the $e+$ and $g+$ optical transitions are allowed since $\langle g|\mu^-|-\rangle = \langle e|\mu^+|-\rangle = 0$. $|+\rangle$ is superradiant, and $|-\rangle$ is a dark state.

Three elements ρ'_{gg}, ρ'_{+g}, and ρ'_{++} determine the state of the dimer after photon emission $\rho' = R\rho(0)$. The time evolution between two emissions is represented by a 3×3 transition matrix $W(\tau) \equiv R\mathcal{U}(\tau)$, which determines the n-time correlation functions:

$$g^{(n)}(\tau_1, \ldots, \tau_{n-1}) = \mathrm{Tr} W(\tau_{n-1}) \ldots W(\tau_2) \cdot W(\tau_1)\rho'. \tag{32}$$

A weak-field expansion of $g^{(2)}$ is given in Appendix E.

We next consider two limiting cases.

(i) *Small dephasing* $\Gamma_\sigma, \Gamma \ll J$. In this case photons emitted from $e+$ and $+g$ transitions are frequency resolved. The coherence ρ_{+g} after detection may be neglected. We then set R_{+ge+}, $R_{g++e} = 0$ and introduce two resetting operators $R^{(e)}(=R_{++ee})$ for the $|e\rangle \to |+\rangle$ and $R^{(+)}(=R_{gg++})$ for the $|+\rangle \to |g\rangle$ photon emissions,

$$g^{(2)}(t) \approx \sum_{ij=e,+} g_{ij}^{(2)}(t).$$

The four two-point correlation functions $g_{pq}^{(2)}$, $p, q = e, +$ represent the joint probabilities to detect a photon q at time 0 and p at t,

$$g_{pq}^{(2)}(t) = \frac{\mathrm{Tr} R^{(p)} \mathcal{U}(t) R^{(q)} \rho(0)}{\mathrm{Tr} \sum_k R^{(k)} \rho(0)}.$$

The asymmetry $g_{e+}^{(2)} \neq g_{+e}^{(2)}$ [see Eqs. (E4) and (E5)] observed in single quantum dots[91,92] reflects multiphoton emission from higher exciton manifolds.[43]

For resonant excitation $\Delta \equiv \omega - \epsilon = -J$

$$g^{(2)}(0) = \frac{\Gamma \hat{\Gamma}_{+g}}{(1 + \gamma/\Gamma)4J^2} \left(\frac{\hat{\Gamma}_{e+}}{\Gamma} - 1 \right), \tag{33}$$

and assuming that $J \gg \Gamma$, $\hat{\Gamma}_{+g}$, $\hat{\Gamma}_{e+}$ the two-exciton manifold is not active, antibunching $g^{(2)}(0) \approx 0$ is observed and all photons come from the one-exciton manifold $g^{(2)} \approx g_{++}^{(2)}$ [Eq. (E5)].

(ii) *Large dephasing* ($\Gamma_\sigma \gg J, \Delta, \gamma$). The dimer has the same steady state and evolution operator as those of two independent chromophores ($g_I^{(2)}, M_I$). However, the resetting procedure assumes an entangled state $|+\rangle$ after emission from $|e\rangle$ so that $g^{(2)}(0) = 2g_I^{(2)}(0)$ [see Eq. (E2)] and drops to half of its initial value after a short dephasing time $t \sim \hat{\Gamma}_{12}^{-1}$, and $g^{(2)}(0+) = g^2(0)/2$ corresponding to two independent chromophores. N independent chromophores are described by taking $\mathcal{L} = \mathcal{L}_1 + \mathcal{L}_2 + \cdots$ and $R = R^{(1)} + R^{(2)} + \cdots$ or $\langle N_n N_m \rangle = \langle N_n \rangle \langle N_m \rangle$. Identical independent chromophores have $g_I^{(2)} \times (t) = 1 + (g_0^{(2)}(t) - 1)/N$ and $M_I(t) = M_0(t)$, where $g_0^{(2)}, M_0(t)$ correspond to the monomer.

(b) *Site resolved emission* may be observed for $|\epsilon_1 - \epsilon_2| \gg J, \Gamma, \hat{\Gamma}$. The coherence ρ_{12} is very small in steady state [Eq. (E6)], so that the emission from the one-exciton manifold is not cooperative and one can introduce a resetting superoperator $R^{(1)}$, $(R^{(2)})$ for photon emission from site $|1\rangle$, $(|2\rangle)$ respectively. At short times $g_{12}^{(2)}(0+) \approx g_{21}^{(2)}(0+) \approx \rho_{ee}/(\rho_{11} + \rho_{22} + \rho_{ee})$. This is different from case (i) where various manifolds are frequency resolved.

(c) *Exciton annihilation* $\gamma \gg J, \Gamma, \Gamma_\sigma$ suppresses the two-exciton population. Antibunching $g^{(2)} \ll 1$ may then be observed even for weak couplings $J \ll \hat{\Gamma}$ [Eq. (E3)],

$$g^{(2)}(0)=\frac{\hat{\Gamma}_{+g}(1+\Gamma/\hat{\Gamma}_{eg})}{\hat{\Gamma}_{e+}(1+\gamma/\Gamma)}. \tag{34}$$

V. MONOMER WITH ARBITRARY FLUCTUATION TIME SCALE

We have calculated $\tilde{\mathcal{U}}(z)$ using a continued fraction expansion of Eq. (23) (see Appendix B).[78,79] Convergence is rapid for fast fluctuations, but higher levels of the hierarchy are required for slow fluctuations ($\sim$1000 levels for $\kappa=0.005$). The steady state density matrix was calculated using Eq. (28). $g^{(2)}$ and M were obtained from Eqs. (20) and (25). The Laplace transform is inverted by fast Fourier transform using discretization of Bromwich integral[93,94]

$$f\left(t=\frac{2\pi k}{\mathcal{N}\delta^{\mathcal{E}}}\right) \approx \mathrm{Re}\exp\left(\frac{2\pi kz}{\mathcal{N}\delta^{\mathcal{E}}}\right) \times\left[\frac{\delta^{\mathcal{E}}}{2\pi}f(z)+\frac{\delta^{\mathcal{E}}}{\pi}\sum_{j=1}^{\mathcal{N}-1}\tilde{f}(z+ij\delta^{\mathcal{E}})\exp\frac{i2\pi jk}{\mathcal{N}}\right], \tag{35}$$

where $\delta^{\mathcal{E}}$ is the length of the integration step in Laplace space, $z>0$ is the distance of integration line from the singularity at $z=0$, and $\mathcal{N}=2^{13}-2^{17}$ is the number of frequencies used for inversion.

$g^{(2)}$ is displayed in the left column of Fig. 2 for various values of κ, holding the linewidth Γ_σ [Eq. (29)] fixed. Panel (A) shows slow ($\kappa=0.005$, solid line) and fast ($\kappa=20$, dashed line) fluctuations. There is a period after a photon emission where a single TLS cannot emit a second photon and $g^{(2)}(0)=0$. $g^{(2)}$ approaches 1 for long times, and $g^{(2)}>1$ is observed for slow fluctuations at intermediate times. The interplay of antibunching and bunching is also observed in M (right column). Sub-Poissonian statistics ($M<0$) is found for arbitrary binning times and fast fluctuations; however, for slow fluctuations and longer binning times bunching dominates resulting in super-Poissonian statistics ($M>0$). For very slow fluctuations a large number of excitations must be accounted for in the simulations, and approximation schemes based on time scale separation (see Appendix F or Ref. 68) should be used. Neglecting short time contributions the Mandel parameter is obtained by combining Eqs. (26) and (F4),

$$M(t)=\frac{2}{F_0}\sum_{\alpha=1}^{\infty}F_\alpha^2\left(\frac{1}{\alpha\Lambda}-\frac{1-e^{-\alpha\Lambda t}}{t\alpha^2\Lambda^2}\right), \tag{36}$$

where F_α represent Lorentzian lineshapes in the Fokker-Planck eigenbasis Eq. (F5). Row (B) shows the variation of photon statistics with detuning for a slow bath. Detuning suppresses the antibunching, and an oscillatory pattern is found for large detuning (solid line). For large detuning and fast and weak fluctuations $(1-\hat{\Gamma}_{eg}/\Gamma)\Delta^2>\hat{\Gamma}^2(1+\hat{\Gamma}_{eg}/\Gamma)$, the statistics becomes super-Poissonian.[55] The inset in the right panel shows that bunching is not suppressed by slow fluctuations even when they are strong ($\Gamma_\sigma\gg\Gamma$). For fast fluctuations (row C) with the same Γ_σ, the Mandel parameter is negative, in agreement with Ref. 55. The effect of slow and fast fluctuations is qualitatively different, since the former cannot be accounted for by simply adding a dephasing rate.

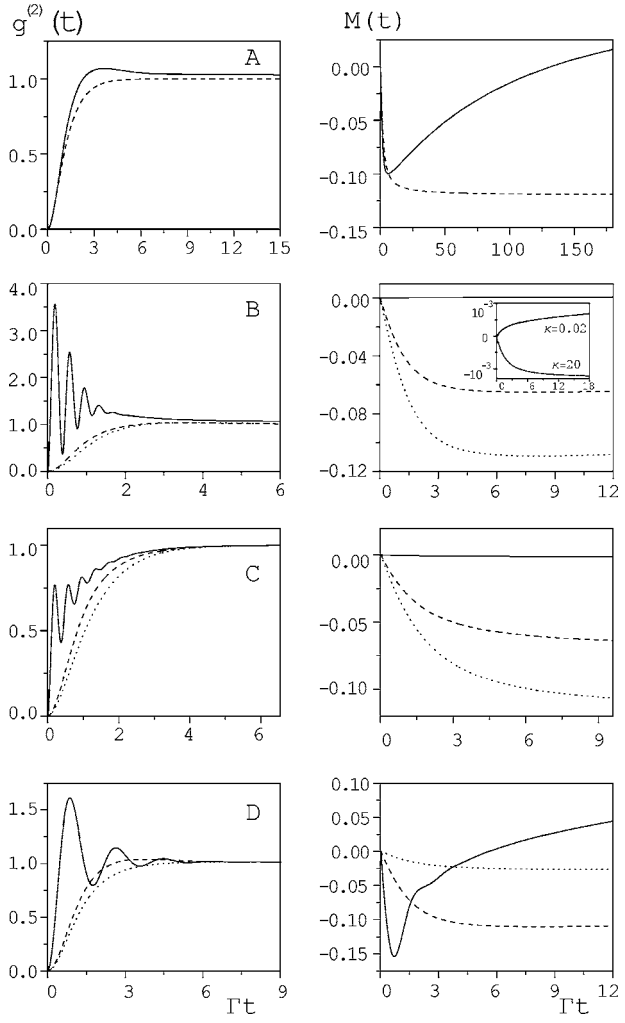

FIG. 2. $g^{(2)}$ (left column) and M (right column) for a monomer. (a) Slow (solid line $\kappa=0.005$) and fast (dashed line $\kappa=20$) bath $\Delta=0.0$, $\Gamma_\sigma=4\Gamma$, $\mathcal{E}=0.5\Gamma$. (b) Variable laser detuning, $\Delta/\Gamma=0.17$, 1.7, and 17Γ (dotted, dashed and solid line), in the slow fluctuation regime $\kappa=0.02$, for $\mathcal{E}=0.5\Gamma$ and $\Gamma_\sigma=4\Gamma$. Inset: M for large detuning and $\Delta/\Gamma=17$ for fast $\kappa=0.02$ vs slow $\kappa=20$ fluctuations. (c) Same as (b) but in fast fluctuation regime $\kappa=20$. (d) Varying Rabi frequency, $\mathcal{E}=0.05$, 0.5, and 3.3Γ (dotted, dashed and solid line), in the slow fluctuation regime $\kappa=1/50$. $\Gamma_\sigma=4\Gamma$ and $\Delta=0$.

The saturation behavior with field intensity in the slow fluctuation regime is demonstrated in row (D). Rabi oscillations and super-Poissonian statistics are seen for strong fields. Note that unlike $g^{(2)}$, M is smaller for strong fields and short binning times. Lowest order perturbative calculations[66] predict that $g^{(2)}$ is independent on $\mathcal{E}$ and $M\propto\mathcal{E}^2$. Our simulations show a nontrivial dependence of photon counting as the Rabi frequency is varied from the weak field (dotted line, $\mathcal{E}=0.1\Gamma$) to the Rabi oscillation regime (solid line, $\mathcal{E}=6.7\Gamma$).

VI. DIMER WITH ARBITRARY FLUCTUATION TIME SCALE

For a dimer, the Hamiltonian Eq. (1) reads

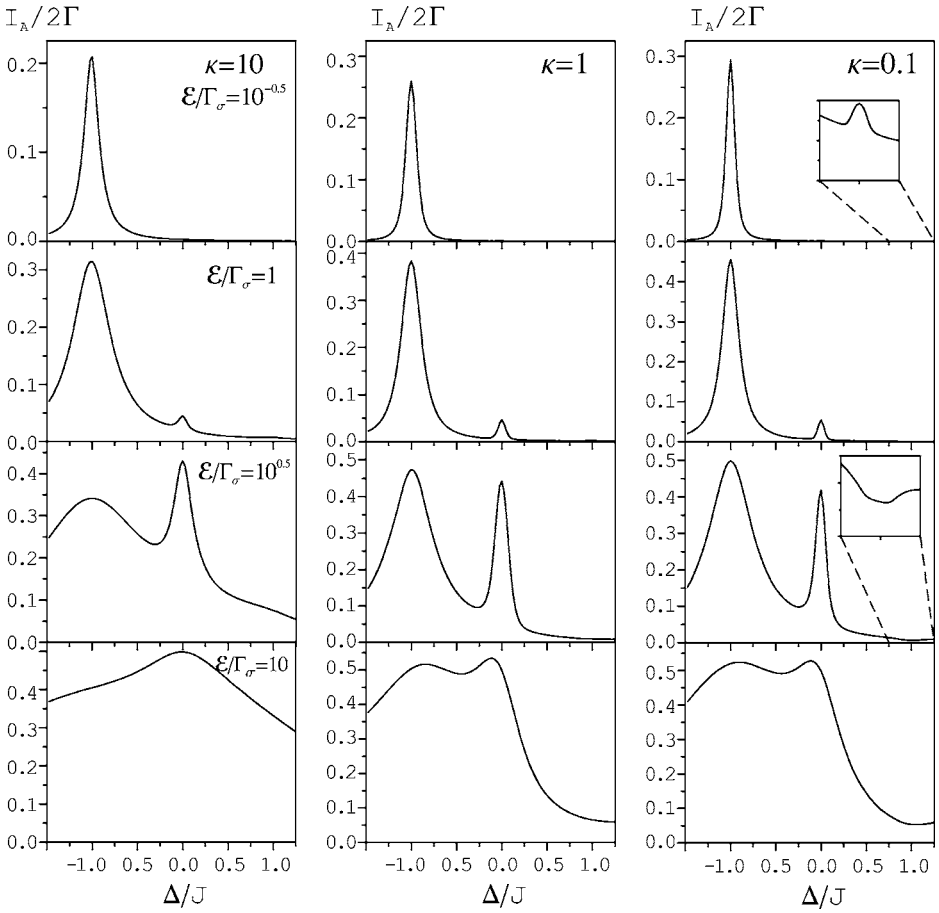

FIG. 3. Strong field absorption lineshapes of dimer. From top to bottom $\mathcal{E}/\Gamma_\sigma=\sqrt{0.1},1,\sqrt{10}$, and 10. From left to right column $\kappa=10$, 1, and 0.1. Insets: Magnified of lineshape at $\Delta=J$, $\Gamma=15\Gamma_\sigma$, and $J/\Gamma_\sigma=10$.

$$H_0=\left(\frac{\epsilon_1+\epsilon_2}{2}\right)(|+\rangle\langle+|+|-\rangle\langle-|)-J(|+\rangle\langle+|-|-\rangle\langle-|)$$

$$+\frac{(\epsilon_1-\epsilon_2)}{2}(|+\rangle\langle-|+|-\rangle\langle+|)+(\epsilon_1+\epsilon_2)|e\rangle\langle e|, \quad (37)$$

and the interaction with the laser field [Eq. (4)] is

$$H_S=H_0-\frac{\mathcal{E}}{\sqrt{2}}(|+\rangle\langle g|+|g\rangle\langle+|+|+\rangle\langle e|+|e\rangle\langle+|). \quad (38)$$

The radiative rates Eq. (6) are

$$\mathcal{K}_{gg++}=\mathcal{K}_{++ee}=\mathcal{K}_{g++e}=\mathcal{K}_{+ge+}=2\Gamma,$$

$$\mathcal{K}_{++++}=\mathcal{K}_{eeee}=\mathcal{K}_{+e+e}=\mathcal{K}_{e+e+}=-2\Gamma,$$

$$\mathcal{K}_{+-+-}=\mathcal{K}_{-+-+}=\mathcal{K}_{+g+g}=\mathcal{K}_{g+g+}$$
$$=\mathcal{K}_{gege}=\mathcal{K}_{egeg}=\mathcal{K}_{e-e-}=\mathcal{K}_{-e-e}=-\Gamma, \quad (39)$$

and the exciton annihilation rates are [85]

$$\gamma_{eeee}=-2\gamma, \quad \gamma_{++ee}=\gamma_{--ee}=\gamma,$$

$$\gamma_{e+e+}=\gamma_{e-e-}=\gamma_{+e+e}=\gamma_{-e-e}=\gamma_{egeg}=\gamma_{gege}=-\gamma. \quad (40)$$

The resetting matrix [Eq. (15)] includes the positive rates of Eq. (39),

$$R_{++ee}=R_{gg++}=R_{+ge+}=R_{g++e}=2\Gamma \quad (41)$$

and $R=0$ otherwise.

In the following simulations we assume independent fluctuations of the two molecules with the same oscillator parameters Γ_σ,κ [Eq. (29)], and $\epsilon_1=\epsilon_2$. The emission [Eq. (21)] is proportional to the absorption [Eq. (22)] as long as exciton annihilation is negligible. Below we display the absorption lineshape for $\gamma=0$ or for weak field $\rho_{ee}/\langle I\rangle\sim 10^{-3}$, where $I_A\approx\langle I\rangle$. The absorption lineshapes [Eq. (22)] for well resolved transitions $J/\Gamma_\sigma=10$ are presented in Fig. 3 for different field strengths $\mathcal{E}$ and fluctuation time scales κ and fixed Γ_σ. Saturation bradening is observed for stronger fields (bottom row) [see Eq. (D5)], in particular, for a fast bath. Slow bath absorption lines are narrower and better resolved. Weak field lineshapes (top) show dominant $g+$ transition at $\Delta=-J$. With increasing field two-photon absorption becomes significant, and finally the lineshape is centered around $\Delta=0$. The $\Delta=J$ peaks are weak (see insets) because the sequential excitation $|g\rangle\rightarrow|+\rangle\rightarrow|e\rangle$ is only relevant for nonresolved lines when both the first and the second steps are possible. For strong fields, two-photon absorption may be more effective than the one-photon $(g+)$ absorption and reversing ρ_{++},ρ_{ee} populations. In this case turning on the $+e$ transition facilitates the induced emission and leads to an absorption dip at $\Delta=J$ (inset at bottom right panel). The effect is observed for a slow bath which has weaker lineshape tails suppressing the $+g$ transition.

We have further simulated $g^{(2)}$, focusing on the short-time dip, which is a measure of cooperativity. In Fig. 4 we depict $g^{(2)}$ for strong dephasing $\hat{\Gamma}_\sigma\gg J$. Panel (A) shows the decay of quantum coherence with varying dephasing rate.

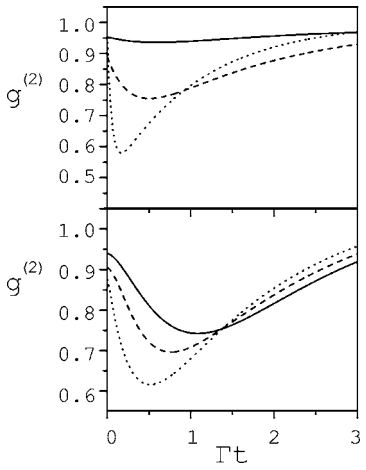

FIG. 4. Fluorescence autocorrelation function [Eq. (20)] of a dimer. Top: Various dephasing rates, $\Gamma_\sigma/\Gamma=0.17$ (solid), 1.7 (dashed), and 17 (dotted line), in the fast fluctuation regime $\kappa=20$. Molecules are weakly coupled, $J=0.03\Gamma$, $\Delta=0$, and $\chi=0.1\Gamma$. Bottom: Varying bath time scales, $\kappa=0.5$ (solid), 1 (dashed), and 10 (dotted line), for $\hat{\Gamma}_\sigma=3.3\Gamma$, $J=0.03\Gamma$, $\Delta=0.0$, and $\mathcal{E}=0.14\Gamma$.

For fast dephasing, the dimer behaves as two independent chromophores with $g^{(2)}(0+)=1/2$, and $g^{(2)}$ is insensitive to the fluctuation time scale. For $\Gamma\approx\Gamma_\sigma$, κ becomes relevant and dephasing is less effective in the slow fluctuation regime, as shown at Fig. 4(b).

Figure 5 compares the effect of the two antibunching mechanisms on the short-time $g^{(2)}$ dip. Panels (A) and (B) show the influence of strong coupling $J\approx\hat{\Gamma}_\sigma$ between chromophores at $\Delta=-J$. The two-exciton state does not participate and the short-time behavior mimics the single chromophore. Notable differences are observed between fast [$\kappa=20$, Fig. 5(a)] and slow [$\kappa=0.5$, Fig. 5(b)] fluctuations, but in both regimes the dip becomes deeper as the coupling is increased.

A similar antibunching is observed for strong exciton-exciton annihilation [Figs. 5(c) and 5(d)]. This is usually the cause of the short-time dip; however, a recent study[49] found a two-photon absorption resonance consistent with the Bloch equation model for the dimer. To separate the effect of exciton annihilation we examined a weakly coupled dimer and found very small differences between slow and fast fluctuations; the annihilation channel is not expected to be influenced by fluctuations.

Figure 6 shows how the variation of the antibunching dip with detuning can be used to distinguish between the two mechanisms. Antibunching caused by strong intermolecular coupling shows strong dependence on detuning (top row), in contrast to the dip caused by exciton-exciton annihilation (bottom row). The lineshapes of both models are similar (inset).

The weak field expansion of $g^{(2)}$ for fast fluctuations [Eq. (E2)] shows transitions to two-exciton state that are not observed in weak field lineshape; e.g., at the two-photon absorption resonance $\Delta=0$, (for $\gamma\neq 0; J\gg\Gamma$) the dimer shows bunching $g^{(2)}\gg 1$ for strong coupling $J\gg\gamma$ but antibunching $g^{(2)}\ll 1$ for strong annihilation $J\ll\gamma$,

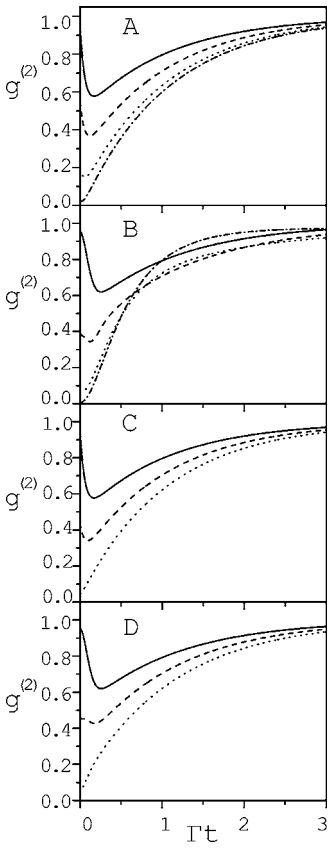

FIG. 5. Fluorescence autocorrelation function for the dimer on resonance. Panels (a) and (b): Varying coupling $J=-\Delta=0.33$, 4.3, 10, and 33Γ for fast ($\kappa=20$) (a) and the slow ($\kappa=0.5$) (b) fluctuations. $\mathcal{E}=0.14\Gamma$, $\hat{\Gamma}_\sigma=17\Gamma$, and $\kappa=0.5$. Panels (c) and (d): Varying two-exciton annihilation rates $\gamma/\Gamma=0$ (solid), 1 (dashed), and 10 (dotted line) for the fast ($\kappa=20$) [panel (c)] and the slow ($\kappa=0.5$) [panel (d)] fluctuations. $J=-\Delta=0.33\Gamma$, $\mathcal{E}=0.14\Gamma$, and $\hat{\Gamma}_\sigma=17\Gamma$.

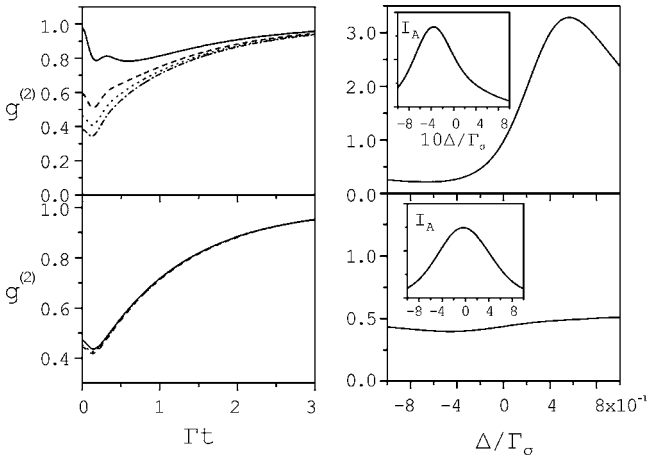

FIG. 6. Left column: Time evolution of $g^{(2)}(t)$ for a dimer. Top panel: Strong intermolecular coupling $J=4.3\Gamma$ for various detuning $\Delta/J=0$ (solid), 1/2 (dashed), 10/13 (dotted), and 1 (dot-dashed line); $\kappa=0.5$; $\mathcal{E}=0.14\Gamma$; $\hat{\Gamma}_\sigma=17\Gamma$; $\gamma=0$. Bottom panel: Exciton annihilation for various detuning $\Delta/J=1$ (dotted), 4 (dashed), and −5.5 (solid line); $\gamma=\Gamma$; $J=0.33\Gamma$; $\kappa=0.5$; $\hat{\Gamma}_\sigma=17\Gamma$; $\mathcal{E}=0.14\Gamma$. Right column: Variation of $g^{(2)}(0)$ with detuning for the models of the left column. Inset: The absorption lineshapes.

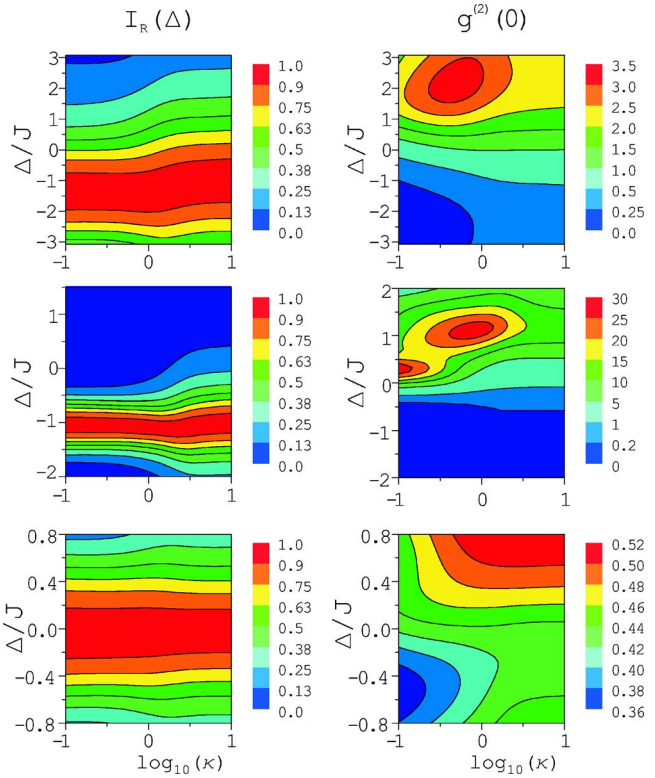

FIG. 7. The absorption lineshape (left) $I_R(\Delta)=I_A(\Delta)/(\max_\Delta I_A(\Delta))$ and $g^{(2)}(0)$ (right) vs Δ and κ. Top: $J=4.3\Gamma$, $\gamma=0$, $\mathcal{E}=0.14\Gamma$, and $\hat{\Gamma}_\sigma=17\Gamma$. Middle: $J=\hat{\Gamma}_\sigma=17\Gamma$, $\gamma=0$, and $\mathcal{E}=0.14\Gamma$. Bottom: $\gamma=\Gamma$, $J=0.33\Gamma$, $\mathcal{E}=0.14\Gamma$, and $\Gamma_\sigma=17\Gamma$.

$$g^{(2)}(0) \approx \frac{J^2\Gamma^2}{(\Gamma+\gamma)\hat{\Gamma}_{+g}^2\hat{\Gamma}_{eg}}. \tag{42}$$

The combined effect of fluctuation time scale and detuning is presented in Fig. 7. The top and middle rows correspond to coupled molecules, the bottom row shows the effect of excitonic annihilation. Left column shows the fluorescence intensity normalized to 1 at the maximum of the lineshape $I_R(\Delta)\equiv I_A(\Delta)/(\max_\Delta I_A(\Delta))$.

For fast fluctuations the maximum fluorescence is at $\Delta=-J$. The lineshape shifts to lower frequencies for slower fluctuations and strong coupling (top and middle row). This effect can be rationalized as level splitting in the static limit, $\sqrt{(\epsilon_1-\epsilon_2)^2+J^2}$ is larger than J, and the lower level still caries most of the oscillator strength. Slower fluctuations show shorter tails as the profile changes from a Lorentzian to a Gaussian.

In the top row the absorption linewidth is larger than the coupling $\Gamma_\sigma/J=4$ so that different absorption lines overlap. $g^{(2)}(0)$ varies significantly with Δ; it is maximized when the excitations to e are resonant and to $+$ are off resonant. As κ is decreased, the shorter lineshape tails may cause more significant variations. As the coupling is increased, $\Gamma_\sigma/J=1$, (middle row) for slow fluctuations the different transitions no longer overlap and a two-exciton absorption peak appears in $g^{(2)}$ near $\Delta\approx 0$. These peaks are observed for weak fields with no saturation broadening unlike the strong field lineshape (Fig. 3) which involves $J\gg\Gamma_\sigma$. This shows the advantage of weak field $g^{(2)}$ measurements.

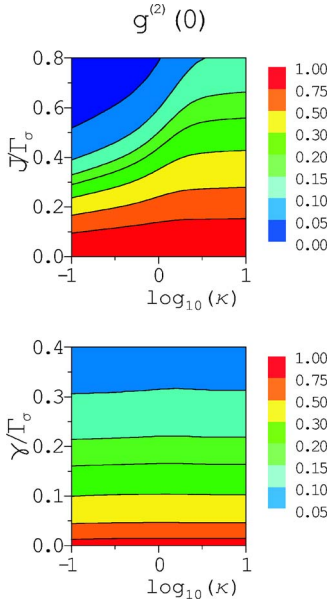

FIG. 8. Top: $g^{(2)}$ vs intermolecular coupling J and κ. $\gamma=0$, $\Delta=-J$, $\mathcal{E}=0.14\Gamma$, and $\Gamma_\sigma=17\Gamma$. Bottom: Two-dimensional plots show $g^{(2)}$ for varying excitonic annihilation rates, γ and κ. $J=0.33\Gamma$, $\Delta=-J$, $\mathcal{E}=0.14\Gamma$, and $\Gamma_\sigma=17\Gamma$.

The absorption peak does not shift with κ when J is small, but otherwise it corresponds to the strong coupling case (top row) since the $+g$ transition dominates the lineshape. In contrast, $g^{(2)}$ for large γ shows antibunching with insignificant variations with Δ,κ as resonant frequencies of all transitions are similar.

In Fig. 8 the fluctuation time scale is varied with intermolecular coupling (top panel) or annihilation rates (bottom panel) for $g^{(2)}$ at $J=-\Delta$. Antibunching is seen in both cases, but only the former depends on the bath time scale.

VII. DISCUSSION

We have studied signatures of spectral diffusion on photon statistics in single molecule spectroscopy of aggregates subjected to Gaussian-Markovian frequency fluctuations. A continued fraction solution of the stochastic Liouville equation is given in Laplace space. The Bloch equations are recovered for fast fluctuations which can be accounted for by simply adding dephasing rates. Bunching ($g^{(2)}>1$ and $M>0$) is seen for slow fluctuations. Detuning may also lead to super-Poissonian statistics which strongly varies with saturation.

Both intermolecular coupling and exciton-exciton annihilation can show a short-time dip in $g^{(2)}$ (antibunching). Exciton annihilation can be distinguished from true cooperativity since it is less sensitive to the fluctuation time scale and detuning. $g^{(2)}$ shows transitions between higher manifolds or two-photon absorption. This information is not contained in the absorption lineshape.

Stochastic models may be generalized by using microscopic models of bath fluctuations. The second factorial moment to fourth order in the electric field may be expressed in terms of six point dipole correlation function.[95] In the high temperature limit it reduces to a four-point function similar

to that found in the semiclassical approach except that the latter contains some spurious contributions which are absent in the exact theory. Another interesting extension will be to introduce non-Markovian stochastic fluctuations described by the continuous-time-random-walk (CTRW) model.[96] Factorial moments may be calculated either using a two-point Green's function for arbitrary Liouville space dynamics with CTRW fluctuations[97] together with the generating function approach or multipoint correlation functions[98] in the perturbative approaches.[66,95]

ACKNOWLEDGMENTS

The support of National Science Foundation (Grant No. CHE 0446555 and EEC 0406750) is gratefully acknowledged. We wish to thank Dr. Thomas la Cour Jansen for the continued fraction routine and valuable discussions.

APPENDIX A: SPECTRUM OF THE FOKKER-PLANCK EQUATION

The eigenvectors of the Fokker-Planck operator Eq. (9) are given by[78]

$$\phi_\alpha = \frac{\exp[-(Q/\sigma)^2/2]}{2^\alpha\sqrt{2\pi}\alpha!\sigma} H_\alpha\left(\frac{Q}{\sigma\sqrt{2}}\right), \tag{A1}$$

where H_α is the nth Hermite polynomial,

$$H_\alpha(x) = (-1)^\alpha e^{x^2}\frac{d^\alpha}{dx^\alpha}e^{-x^2},$$

with eigenvalue $-\alpha\Lambda$. The matrix representation of bath densities and evolution matrices refers to the basis $\{\phi_\alpha\}$, $\alpha=0,1,2,\ldots$. The matrix elements of $\mathcal{L}_B$ are

$$(\mathcal{L}_B)_{\beta,\alpha} = -\alpha\Lambda\delta_{\alpha,\beta}. \tag{A2}$$

The Q variable is represented by the tridiagonal matrix,

$$(Q)_{\beta\alpha} = \beta\sigma\sqrt{2}\delta_{\beta,\alpha+1} + \frac{\sigma}{\sqrt{2}}\delta_{\beta,\alpha-1}. \tag{A3}$$

Greek indices denote bath degrees of freedom.

Note that integration over bath variables is achieved by taking the zero (bath) component, e.g., the expression for the generating function Eq. (17) reads

$$\bar{\mathcal{G}}(t,s) = \langle\langle \mathrm{Tr}\mathcal{G}(t;s)\rho(0)\rangle\rangle = \mathrm{Tr}\sum_\alpha \mathcal{G}(t;s)_{0,\alpha}\rho_\alpha(0). \tag{A4}$$

APPENDIX B: CONTINUED FRACTION EXPANSION OF THE FOKKER-PLANCK EQUATION

General discussion of continued fraction expansions is given in Refs. 78 and 79. Below we briefly present the basic results for tridiagonal matrices, which are required to describe linear coupling to bath,

$$A = \begin{pmatrix} \mathcal{Q}_0 & \mathcal{Q}_0^+ & 0 & 0 & \ldots & \ldots \\ \mathcal{Q}_1^- & \mathcal{Q}_1 & \mathcal{Q}_1^+ & 0 & \ldots & \ldots \\ \ldots & \ldots & \ldots & \ldots & \ldots & \ldots \\ 0 & \ldots & \mathcal{Q}_\alpha^- & \mathcal{Q}_\alpha & \mathcal{Q}_\alpha^+ & \ldots \\ \ldots & \ldots & \ldots & \ldots & \ldots & \ldots \end{pmatrix}.$$

The inverse $A^{-1}=\mathcal{G}$ is determined by the off diagonal $\alpha\neq\beta$ equations,

$$\mathcal{Q}_\alpha^-\mathcal{G}_{\alpha-1,\beta} + \mathcal{Q}_\alpha\mathcal{G}_{\alpha,\beta} + \mathcal{Q}_\alpha^+\mathcal{G}_{\alpha+1,\beta} = 0, \tag{B1}$$

as well as diagonal equations,

$$\mathcal{Q}_\alpha^-\mathcal{G}_{\alpha-1,\alpha} + \mathcal{Q}_\alpha\mathcal{G}_{\alpha,\alpha} + \mathcal{Q}_\alpha^+\mathcal{G}_{\alpha+1,\alpha} = 1. \tag{B2}$$

Eq. (B1) is independent of the β variable. Consequently we can introduce $\mathcal{S}^+,\mathcal{S}^-$ matrices,

$$\mathcal{G}_{\alpha\pm1,\beta} = \mathcal{S}_\alpha^\pm\mathcal{G}_{\alpha,\beta}.$$

Using Eq. (B1) these matrices may be solved iteratively,

$$S_\alpha^\pm = \frac{-1}{\mathcal{Q}_{\alpha\pm1} + \mathcal{Q}_{\alpha\pm1}^\pm\mathcal{S}_{\alpha\pm1}^\pm}\mathcal{Q}_{\alpha\pm1}^\mp. \tag{B3}$$

Combined with Eq. (B2) it yields for the diagonal terms,

$$\mathcal{G}_{\alpha,\alpha} = \frac{1}{\mathcal{Q}_\alpha^-\mathcal{S}_\alpha^- + \mathcal{Q}_\alpha + \mathcal{Q}_\alpha^+\mathcal{S}_\alpha^+},$$

while the off-diagonal terms can be calculated from (B3).

Using Eq. (A3) we can specify these matrices for a single Brownian oscillator,

$$\mathcal{Q}_\alpha = z - \mathcal{L}_S + (1-s)R + \alpha\Lambda,$$

$$\mathcal{Q}_\alpha^+ = -\sqrt{2}(\alpha+1)\sigma D, \tag{B4}$$

$$\mathcal{Q}_\alpha^- = -\frac{\sigma}{\sqrt{2}}D\ \mathrm{sign}(\alpha).$$

Many applications (e.g., fast limit) only require the 0,0 term,

$$\mathcal{G}_{0,0} = \cfrac{1}{\mathcal{Q}_0 - \mathcal{Q}_0^+\cfrac{1}{\mathcal{Q}_1 - \mathcal{Q}_1^+\cfrac{1}{\mathcal{Q}_2 - \mathcal{Q}_2^+\cfrac{1}{\ldots}\mathcal{Q}_3^-}\mathcal{Q}_2^-}\mathcal{Q}_1^-}. \tag{B5}$$

Combining Eq. (B5) with Eq. (B4) gives Eq. (30).

APPENDIX C: STATISTICAL MOMENTS OF PHOTON COUNTING

We consider a stationary process where a time independent Liouville superoperator can be written in a proper basis. The starting point is the perturbative series of Eq. (23) in $\delta s = s-1$,

$$\frac{1}{z-\mathcal{L}-\delta sR} = \sum_{k=0}^\infty \frac{1}{z-\mathcal{L}}\left(\delta sR\frac{1}{z-\mathcal{L}}\right)^k. \tag{C1}$$

The calculation of M [Eq. (19)] requires the first two derivatives,

$$\left.\frac{\partial}{\partial s}\tilde{\mathcal{G}}(z;s)\right|_{s=1}=\frac{1}{z-\mathcal{L}}R\frac{1}{z-\mathcal{L}},$$

$$\left.\frac{\partial^2}{\partial s^2}\tilde{\mathcal{G}}(z;s)\right|_{s=1}=2\frac{1}{z-\mathcal{L}}R\frac{1}{z-\mathcal{L}}R\frac{1}{z-\mathcal{L}}. \tag{C2}$$

The Liouville superoperator may be formally decomposed as

$$\mathcal{L}=\sum_{q=0}^{\infty}|L_q\rangle\rangle\xi_q\langle\langle S_q|, \tag{C3}$$

where $|L_q\rangle\rangle$ is left eigenvector and $\langle\langle S_q|$ is right eigenvector for eigenvalue ξ_q ($\xi_0=0$). The evolution superoperator, the steady state, and the tracing operation are represented by

$$\tilde{\mathcal{U}}(z)=\sum_{q=0}^{\infty}|L_q\rangle\rangle\frac{1}{z-\xi_q}\langle\langle S_q|,\quad \rho(0)=|L_0\rangle\rangle,$$

$$\langle\langle S_0|\ldots=\langle\langle \mathrm{Tr}\ldots\rangle\rangle. \tag{C4}$$

Straightforward calculation gives

$$\tilde{\mathcal{U}}(z)|L_0\rangle\rangle=\frac{1}{z}|L_0\rangle\rangle,\quad \langle\langle S_0|\tilde{\mathcal{U}}(z)=\frac{1}{z}\langle\langle S_0|. \tag{C5}$$

Combining Eqs. (C5), (C2), and (C4) we get Eq. (25).

The decomposition Eq. (C4) determines the most general form of M for stochastic Liouville model,

$$M(t)=\frac{-2}{\langle\langle S_0|R|L_0\rangle\rangle}\sum_{q=1}^{\infty}\langle\langle S_0|R|L_q\rangle\rangle\langle\langle S_q|R|L_0\rangle\rangle\times\left(\frac{1}{\xi_q}+\frac{1-e^{\xi_q t}}{t\xi_q^2}\right). \tag{C6}$$

The summation does not include $q=0$ which is exactly subtracted. Equation (C6) give a solution for asymptotic Mandel parameter. We rearrange this rather formal result to a form which is more convenient for calculation,

$$M(\infty)=\frac{-2}{\langle\langle S_0|R|L_0\rangle\rangle}\sum_{q=1}^{\infty}\langle\langle S_0|R|L_q\rangle\rangle\frac{1}{\xi_q}\langle\langle S_q|R|L_0\rangle\rangle=\frac{2}{\langle\langle \mathrm{Tr}R\rho(0)\rangle\rangle}\lim_{\delta\to 0}\mathrm{Re}\left\langle\!\!\left\langle \mathrm{Tr}\,R\frac{1}{i\delta-\mathcal{L}}R\rho(0)\right\rangle\!\!\right\rangle, \tag{C7}$$

where we used $\mathrm{Re}(\langle\langle S_0|R|L_0\rangle\rangle\langle\langle S_0|R|L_0\rangle\rangle/i\delta)=0$, Eq. (C3), and the contributions $q\geqslant 1$ in Eq. (C6) that are continuous at $\delta=0$.

Based on the central limit theorem we expect a Gaussian distribution of photons at long times. Instead of using the central limit theorem one may directly prove that the higher moments are consistent with a Gaussian distribution. Let us consider the third moment,

$$\begin{aligned}\langle(n-\langle n\rangle)^3\rangle&=\langle n(n-1)(n-2)\rangle+3\langle n(n-1)\rangle(1-\langle n\rangle)+2\langle n\rangle^3-3\langle n\rangle^2+\langle n\rangle\\&=\langle\langle S_0|R|L_0\rangle\rangle\left[t+6\sum_{q=1}^{\infty}\left(2\frac{e^{\xi_q t}-1}{\xi_q^3}-t\frac{e^{\xi_q t}+1}{\xi_q^2}\right)\langle\langle S_0|R|L_q\rangle\rangle\langle\langle S_q|R|L_0\rangle\rangle\right]+6\sum_{q,q'=1}^{\infty}\langle\langle S_0|R|L_q\rangle\rangle\langle\langle S_q|R|L_{q'}\rangle\rangle\langle\langle S_{q'}|R|L_0\rangle\rangle\\&\quad\times\frac{1}{\xi_q-\xi_{q'}}\left(\frac{e^{\xi_q t}-1}{\xi_q^2}-\frac{t}{\xi_q}+\frac{t}{\xi_{q'}}-\frac{e^{\xi_{q'}t}-1}{\xi_{q'}^2}\right)+6\sum_{q=1}^{\infty}\left(\frac{e^{\xi_q t}-1}{\xi_q^2}-\frac{t}{\xi_q}\right)\langle\langle S_0|R|L_q\rangle\rangle\langle\langle S_q|R|L_0\rangle\rangle,\end{aligned}$$

it grows at most linearly with t, so by fixing the mean and variance as in the central limit theorem the deviations from Gaussian vanishes as $1/\sqrt{t}$.

APPENDIX D: PHOTON COUNTING IN A MONOMER

A single two-level molecule interacting with an intense resonant monochromatic laser is described in the interaction representation Eq. (2) by the Hamiltonian,

$$H_S=\epsilon\hat{B}^{\dagger}B-\tfrac{1}{2}\mathcal{E}(B^{\dagger}+B), \tag{D1}$$

where ϵ is the transition frequency, $\mathcal{E}$ is the Rabi frequency, and ω is the laser frequency.

We use the real variables $\rho_{eg}=\rho'_{eg}+i\rho''_{eg}$. The time evolution of density matrix is described by

$$\frac{\partial}{\partial t}\begin{pmatrix}\rho_{ee}\\ \rho_{gg}\\ \rho'_{eg}\\ \rho''_{eg}\end{pmatrix}=\begin{pmatrix}-\Gamma & 0 & 0 & \mathcal{E}\\ \Gamma & 0 & 0 & -\mathcal{E}\\ 0 & 0 & -\Gamma/2 & -\Delta\\ -\mathcal{E}/2 & \mathcal{E}/2 & +\Delta & -\Gamma/2\end{pmatrix}\begin{pmatrix}\rho_{ee}\\ \rho_{gg}\\ \rho'_{eg}\\ \rho''_{eg}\end{pmatrix}, \tag{D2}$$

where Γ is the radiative rate, and $\Delta=\omega-\epsilon-Q$ is the detuning.

The resetting matrix is

$$R=\begin{pmatrix}0&0&0&0\\ \Gamma&0&0&0\\ 0&0&0&0\\ 0&0&0&0\end{pmatrix}.$$

For fast bath at resonance $\Delta=0$, the steady state density matrix is

$$\rho_{ee}=\frac{\mathcal{E}^2}{2(\mathcal{E}^2+\Gamma\hat{\Gamma}_{eg})},\quad \rho_{gg}=\frac{\mathcal{E}^2+2\Gamma\hat{\Gamma}_{eg}}{2(\mathcal{E}^2+\Gamma\hat{\Gamma}_{eg})},$$
$$\rho_{eg}=\frac{i\Gamma\mathcal{E}}{2(\mathcal{E}^2+\Gamma\hat{\Gamma}_{eg})}.$$

In the overdamped limit $|\hat{\Gamma}_{eg}-\Gamma|>2\mathcal{E}$ we get

$$g^{(2)}(t)=1-\frac{1}{2}\left[\left(1+\frac{\Gamma+\hat{\Gamma}_{eg}}{\Xi}\right)e^{-(\Gamma+\hat{\Gamma}_{eg}-\Xi)t/2}+\left(1-\frac{\Gamma+\hat{\Gamma}_{eg}}{\Xi}\right)e^{-(\Gamma+\hat{\Gamma}_{eg}+\Xi)t/2}\right]$$

and

$$M(t)=-\frac{\Gamma\mathcal{E}^2}{t(\Gamma\hat{\Gamma}_{eg}+\mathcal{E}^2)}\left[\frac{t(\Gamma+\hat{\Gamma}_{eg})}{\Gamma\hat{\Gamma}_{eg}+\mathcal{E}^2}-\frac{\Gamma^2+\hat{\Gamma}_{eg}\Gamma+\hat{\Gamma}_{eg}^2-\mathcal{E}^2}{(\Gamma\hat{\Gamma}_{eg}+\mathcal{E}^2)^2}+\frac{(\Gamma+\hat{\Gamma}_{eg}+\Xi)e^{-(\Gamma+\hat{\Gamma}_{eg}-\Xi)t/2}}{\Xi(\Gamma^2+\hat{\Gamma}_{eg}^2-2\mathcal{E}^2)-\Xi^2(\Gamma+\hat{\Gamma}_{eg})}+\frac{(\Gamma+\hat{\Gamma}_{eg}-\Xi)e^{-(\Gamma+\hat{\Gamma}_{eg}+\Xi)t/2}}{\Xi(\Gamma^2+\hat{\Gamma}_{eg}^2-2\mathcal{E}^2)+\Xi^2(\Gamma+\hat{\Gamma}_{eg})}\right],\tag{D3}$$

where $\Xi=\sqrt{(\hat{\Gamma}_{eg}-\Gamma)^2-4\mathcal{E}^2}$.

In the Rabi oscillation regime $|\hat{\Gamma}_{eg}-\Gamma|<2\mathcal{E}$ we have

$$g^{(2)}(t)=1-e^{-(\Gamma+\hat{\Gamma}_{eg})t/2}\left[\cos(\Xi t/2)+\frac{\Gamma+\hat{\Gamma}_{eg}}{\Xi}\sin(\Xi t/2)\right]$$

and

$$M(t)=-\frac{\Gamma\mathcal{E}^2}{t(\Gamma\hat{\Gamma}_{eg}+\mathcal{E}^2)}\left\{\frac{t(\Gamma+\hat{\Gamma}_{eg})}{\Gamma\hat{\Gamma}_{eg}+\mathcal{E}^2}-\frac{\Gamma^2+\hat{\Gamma}_{eg}\Gamma+\hat{\Gamma}_{eg}^2-\mathcal{E}^2}{(\Gamma\hat{\Gamma}_{eg}+\mathcal{E}^2)^2}+\frac{e^{-(\Gamma+\hat{\Gamma}_{eg})t/2}}{(\Gamma\hat{\Gamma}_{eg}+\mathcal{E}^2)^2}\times\left[(\Gamma^2+\hat{\Gamma}_{eg}\Gamma+\hat{\Gamma}_{eg}^2-\mathcal{E}^2)\cos(\Xi t/2)-\frac{(\Gamma+\hat{\Gamma}_{eg})}{\Xi}(\Gamma^2-\hat{\Gamma}_{eg}\Gamma+\hat{\Gamma}_{eg}^2-3\mathcal{E}^2)\sin(\Xi t/2)\right]\right\}\tag{D4}$$

where $\Xi=\sqrt{4\mathcal{E}^2-(\hat{\Gamma}_{eg}-\Gamma)^2}$.

The nonresonant steady state densities are

$$\rho_{ee}=\frac{\mathcal{E}^2}{2(\mathcal{E}^2+\Gamma\hat{\Gamma}_{eg}+\Delta^2\Gamma/\hat{\Gamma}_{eg})},\quad \rho_{gg}=1-\rho_{ee},$$
$$\rho_{eg}=\left(i-\frac{\Delta}{\hat{\Gamma}_{eg}}\right)\frac{\Gamma}{\mathcal{E}}\rho_{ee}.\tag{D5}$$

The lineshape is Lorentzian with linewidth $\hat{\Gamma}_{eg}\sqrt{1+\mathcal{E}^2/\Gamma\hat{\Gamma}_{eg}}$.

The nonresonant autocorrelation function in the weak field limit is

$$g^{(2)}=1+\frac{(\Gamma-\hat{\Gamma}_{eg})(\hat{\Gamma}_{eg}^2+\Delta^2)e^{-\Gamma t}-\{[\hat{\Gamma}_{eg}(\Gamma-\hat{\Gamma}_{eg})+\Delta^2]\cos(\Delta t)+\Delta(2\hat{\Gamma}_{eg}-\Gamma)\sin(\Delta t)\}\Gamma e^{-\hat{\Gamma}_{eg}t}}{\hat{\Gamma}_{eg}[(\Gamma-\hat{\Gamma}_{eg})^2+\Delta^2]}.\tag{D6}$$

APPENDIX E: DIMER IN THE FAST FLUCTUATION LIMIT

We first investigate the strong coupling case by setting $\epsilon_1=\epsilon_2$. The leading terms of the steady state density matrix in the weak field expansion are

$$\rho_{gg}=1,\quad \rho_{+g}=\frac{i\sqrt{2}\mathcal{E}}{2[\hat{\Gamma}_{+g}-i(\Delta+J)]},$$
$$\rho_{--}=\rho_{++}=\frac{\mathcal{E}^2\hat{\Gamma}_{+g}}{2\Gamma(\hat{\Gamma}_{+g}^2+(\Delta+J)^2)},$$
$$\rho_{eg}=\frac{-\mathcal{E}^2}{2[\hat{\Gamma}_{+g}-i(\Delta+J)][\hat{\Gamma}_{eg}-2i\Delta]},$$
$$\rho_{e+}=\frac{i\sqrt{2}\mathcal{E}^3\hat{\Gamma}_{+g}}{4\Gamma[\hat{\Gamma}_{e+}+i(J-\Delta)](\hat{\Gamma}_{+g}^2+(\Delta+J)^2)}+\frac{i\sqrt{2}\mathcal{E}^3}{4[\hat{\Gamma}_{e+}+i(J-\Delta)][\hat{\Gamma}_{+g}-i(\Delta+J)][\hat{\Gamma}_{eg}-2i\Delta]},$$
$$\rho_{ee}=\frac{\mathcal{E}^4}{4(\Gamma+\gamma)[\hat{\Gamma}_{e+}^2+(\Delta-J)^2][\hat{\Gamma}_{+g}^2+(\Delta+J)^2]}\times\left(\frac{\hat{\Gamma}_{e+}\hat{\Gamma}_{+g}}{\Gamma}+\frac{\hat{\Gamma}_{e+}[\hat{\Gamma}_{+g}\hat{\Gamma}_{eg}-2(\Delta+J)\Delta]}{[\hat{\Gamma}_{eg}^2+4\Delta^2]}+\frac{(J-\Delta)[2\Delta\hat{\Gamma}_{+g}+(\Delta+J)\hat{\Gamma}_{eg}]}{[\hat{\Gamma}_{eg}^2+4\Delta^2]}\right).\tag{E1}$$

The second and the third terms in parenthesis of Eq. (32) are connected with two-photon absorption and become negligible with stronger fluctuations. The dephasing rates $\hat{\Gamma}$ correspond to

$$\hat{\Gamma}_{+g}=\Gamma+\frac{\sigma^2}{\Lambda},\quad \hat{\Gamma}_{eg}=\Gamma+\gamma+2\frac{\sigma^2}{\Lambda},$$
$$\hat{\Gamma}_{e+}=2\Gamma+\gamma+\frac{\sigma^2}{\Lambda},\quad \hat{\Gamma}_{12}=2\sigma^2/\Lambda. \tag{E2}$$

The probability of simultaneous emission of two photons is related to the steady state density matrix $\rho(0)$,

$$g^{(2)}(0)=\frac{\rho_{ee}}{(\rho_{ee}+\rho_{++})^2}.$$

For weak fields this gives $g^{(2)}(0)\approx\rho_{ee}/\rho_{++}^2$. The fluorescence maximum is obtained when the laser is resonant with the symmetric state ($\Delta=-J$). In this case

$$g^{(2)}(0)=\frac{\Gamma\hat{\Gamma}_{+g}}{(1+\gamma/\Gamma)(\hat{\Gamma}_{e+}^2+4J^2)}\left(\frac{\hat{\Gamma}_{e+}}{\Gamma}+\frac{\hat{\Gamma}_{e+}\hat{\Gamma}_{eg}-4J^2}{\hat{\Gamma}_{eg}^2+4J^2}\right), \tag{E3}$$

which for $J>>\Gamma,\hat{\Gamma}$ gives Eq. (33). The same steps for $\Delta=0$ gives Eq. (42).

$g^{(2)}$ to leading (fourth) order in the electric field has three types of contributions. We denote $\Theta\equiv\sqrt{\Gamma^2+\hat{\Gamma}_{12}^2}$ and $\Xi\equiv\Gamma_{+g}-i(\Delta+J)$. The first contribution corresponds to $|e\rangle\rightarrow|+\rangle\rightarrow|g\rangle$ emission history,

$$g_{+e}(t)=\frac{\rho_{ee}(0)}{2\rho_{++}^2(0)}\left(\left(1-\frac{\Gamma}{\Theta}\right)\exp[(-\Gamma-\hat{\Gamma}_{12}+\Theta)t]+\left(1+\frac{\Gamma}{\Theta}\right)\exp[(-\Gamma-\hat{\Gamma}_{12}-\Theta)t]\right). \tag{E4}$$

The second contribution is connected to two $w|+\rangle\rightarrow|g\rangle$ emissions,

$$g_{++}(t)=\frac{\mathcal{E}^2\rho_{++}(0)}{4\rho_{++}^2(0)}\times\left(\frac{1}{\Gamma\Xi}+\frac{(\Theta-\Gamma)\exp(-\Gamma-\hat{\Gamma}_{12}+\Theta)t}{\Theta(\Gamma+\hat{\Gamma}_{12}-\Theta)(\Gamma+\hat{\Gamma}_{12}-\Theta-\Xi)}+\frac{(\Theta+\Gamma)\exp(-\Gamma-\hat{\Gamma}_{12}-\Theta)t}{\Theta(\Gamma+\hat{\Gamma}_{12}+\Theta)(\Gamma+\hat{\Gamma}_{12}+\Theta-\Xi)}-\frac{2(\hat{\Gamma}_{12}-\Xi)\exp[-\Xi t]}{\Xi[(\Gamma+\hat{\Gamma}_{12}-\Xi)^2-\Theta^2]}\right)+\text{c.c.} \tag{E5}$$

The third contribution $\delta g^{(2)}\equiv g^{(2)}-\Sigma_{pq=+,e}g_{pq}^{(2)}$ coming from the coherence between $|e\rangle$ and $|g\rangle$ after emission, cannot be attributed to a particular (Hilbert space) emission history and should become negligible when the emission from the one-exciton manifold is frequency resolved from the two-exciton manifold:

$$\delta g^{(2)}(t)=\frac{i\sqrt{2}\mathcal{E}\rho_{e+}(0)}{4\Theta\rho_{++}^2(0)}\left[\frac{(\Theta-\Gamma)}{(\Gamma+\hat{\Gamma}_{12}-\Theta-\Xi)}\times\exp[(-\Gamma-\hat{\Gamma}_{12}+\Theta)t]+\frac{(\Theta+\Gamma)}{(\Gamma+\hat{\Gamma}_{12}+\Theta-\Xi)}\times\exp[(-\Gamma-\hat{\Gamma}_{12}-\Theta)t]-\left(\frac{(\Theta-\Gamma)}{\Gamma+\hat{\Gamma}_{12}-\Theta-\Xi}+\frac{(\Theta+\Gamma)}{(\Gamma+\hat{\Gamma}_{12}+\Theta-\Xi)}\right)\exp[-\Xi t]\right]+\text{c.c.}$$

For weak coupling with the well resolved transitions $|\epsilon_1-\epsilon_2|\gg J,\Gamma,\hat{\Gamma}$ we set $J=0$ denoting that $\Delta_j=\omega-\epsilon_j$, and expand in $\Gamma/|\epsilon_1-\epsilon_2|$ (to first order) to get

$$\rho_{gg}=1,\quad \rho_{jg}=\frac{i\mathcal{E}/2}{\hat{\Gamma}_{jg}-i\Delta_j},$$
$$\rho_{22}=\frac{\mathcal{E}^2}{4\Gamma}\left[\frac{1}{\hat{\Gamma}_{2g}+i\Delta_2}+\frac{1}{\hat{\Gamma}_{2g}-i\Delta_2}-\frac{i\Gamma}{2(\epsilon_2-\epsilon_1)}\left(\frac{1}{\hat{\Gamma}_{2g}+i\Delta_2}-\frac{1}{\hat{\Gamma}_{2g}-i\Delta_2}+\frac{1}{\hat{\Gamma}_{1g}-i\Delta_1}-\frac{1}{\hat{\Gamma}_{1g}+i\Delta_1}\right)\right],$$
$$\rho_{12}=\frac{\mathcal{E}^2}{4\Gamma}\frac{i\Gamma}{2(\epsilon_2-\epsilon_1)}\left[\frac{1}{\hat{\Gamma}_{2g}+i\Delta_2}+\frac{1}{\hat{\Gamma}_{1g}-i\Delta_1}-\frac{1}{\hat{\Gamma}_{2g}-i\Delta_2}-\frac{1}{\hat{\Gamma}_{1g}+i\Delta_1}\right],$$
$$\rho_{eg}=-\frac{\mathcal{E}^2}{4(\hat{\Gamma}_{eg}-i\Delta_1-i\Delta_2)}\left(\frac{1}{\hat{\Gamma}_{1g}-i\Delta_1}+\frac{1}{\hat{\Gamma}_{2g}-i\Delta_2}\right), \tag{E6}$$
$$\rho_{e1}=\frac{i\mathcal{E}^3}{8(\hat{\Gamma}_{e1}+i\Delta_2)}\left[\frac{1}{\Gamma}\left(\frac{1}{\hat{\Gamma}_{1g}+i\Delta_1}+\frac{1}{\hat{\Gamma}_{1g}-i\Delta_1}\right)+\frac{1}{\hat{\Gamma}_{eg}-i\Delta_1-i\Delta_2}\left(\frac{1}{\hat{\Gamma}_{1g}-i\Delta_1}+\frac{1}{\hat{\Gamma}_{2g}-i\Delta_2}\right)\right],$$

$$\rho_{e2}=\frac{i\mathcal{E}^3}{8(\hat{\Gamma}_{e2}+i\Delta_1)}\left[\frac{1}{\Gamma}\left(\frac{1}{\hat{\Gamma}_{2g}+i\Delta_2}+\frac{1}{\hat{\Gamma}_{2g}-i\Delta_2}\right)+\frac{1}{\hat{\Gamma}_{eg}-i\Delta_1-i\Delta_2}\left(\frac{1}{\hat{\Gamma}_{1g}-i\Delta_1}+\frac{1}{\hat{\Gamma}_{2g}-i\Delta_2}\right)\right],$$

$$\rho_{ee}=\frac{i\mathcal{E}}{4(\Gamma+\gamma)}[\rho_{e2}+\rho_{e1}-\rho_{1e}-\rho_{2e}].$$

APPENDIX F: TIME-SCALE SEPARATION

We assume two separated relaxation time scales, fast relaxation of electronic degrees of freedom (with fixed environment) and slow for environment relaxation. At short times we average over the static bath variables, and at long times we assume instantaneous relaxation of system variables. Similar approximations were employed in investigations of dynamic lineshapes and calculations of $g^{(2)}$ for spectral diffusion TLS model[20] and factorial moments.[57]

For a static environment (fixed Q_u) we define the local operators $\mathcal{U}(t,Q_u)\equiv\exp(\mathcal{L}_S+\mathcal{L}_{S-B}(Q_u))t$, the local steady state $\rho(0,Q_u)\equiv\mathcal{U}(t=\infty,Q_u)$, and the local system density matrix after the detection of the first photon $\rho_S(t,Q_u)\equiv\mathcal{U}(t,Q_u)R\rho(0,Q_u)$.

The total density matrix is then obtained as

$$\rho(t)=\rho_S(t,Q_u)\prod_u\rho_B(Q_u).$$

The fast relaxation component is given by

$$g^{(2)}(t)=\frac{\Pi_u(\int_{-\infty}^{\infty}dQ_u\rho_B(Q_u))\mathrm{Tr}R\rho_S(t,Q_u)}{[\Pi_u(\int_{-\infty}^{\infty}dQ_u\rho_B(Q_u))\mathrm{Tr}\rho_S(0,Q_u)]^2}. \tag{F1}$$

To calculate the slow component of relaxation we assume instantaneous local equilibration of system variables; all time evolution is in bath densities,

$$g^{(2)}(t)=\frac{\Pi_u(\int_{-\infty}^{\infty}dQ_u\rho_B(Q_u)\int_{-\infty}^{\infty}dQ_u'P(Q_u';Q_u;t))\mathrm{Tr}\rho_S(0,Q_u')\mathrm{Tr}\rho_S(0,Q_u)}{[\Pi_u(\int_{-\infty}^{\infty}dQ_u\rho_B(Q_u))\mathrm{Tr}\rho_S(0,Q_u)]^2}, \tag{F2}$$

where

$$P(Q_u';Q_u;t)\equiv\frac{1}{\sigma_u\sqrt{2\pi(1-e^{-2\Lambda t})}}\exp\left[\frac{-(Q_u'-e^{-\Lambda t}Q_u)^2}{2\sigma_u^2(1-e^{-2\Lambda t})}\right] \tag{F3}$$

is the Fokker-Planck propagator.[78] Equation (F1) for $t=\infty$ agrees with Eq. (F2) for $t=0$ so that the solutions are concurrent. The long-time solution asymptotically converge to 1 as expected. The Mandel parameter can be finally calculated by combining Eqs. (26), (F1), and (F2). This approximation is similar to algorithm of Ref. 68 which applied time scale separation to calculate factorial moments.

For the monomer, $\rho_s(0,Q)$ is given by Eq. (D5) replacing Δ for $\Delta-Q$, and Eq. (F2) can be recasted in Fokker-Plack eigenbasis Eq. (A1),

$$g^{(2)}=\frac{1}{F_0^2}\sum_{\alpha=0}^{\infty}F_\alpha^2\exp(-\alpha\Lambda t), \tag{F4}$$

where

$$F_\alpha=\frac{\mathcal{E}^2}{2(\mathcal{E}^2+\Gamma\hat{\Gamma}_{eg})}\int_{-\infty}^{\infty}\frac{\phi_\alpha(Q,\sigma)}{1+A(\Delta-Q)^2}dQ, \tag{F5}$$

$$A=\Gamma/(\hat{\Gamma}_{eg}\mathcal{E}^2+\Gamma\hat{\Gamma}_{eg}^2).$$

Equation (36) is obtained by neglecting the short-time antibunching and by applying (26) to long-scale solution Eq. (F4).

[1] A. S. Davydov, *Theory of Molecular Excitons* (McGraw-Hill, New York, 1962).
[2] E. A. Silinsh and V. Čápek, *Organic Molecular Crystals: Interaction, Localization, and Transport Phenomena* (AIP, New York, 1994).
[3] M. Pope and C. E. Swenberg, *Electron Processes in Organic Crystals* (Oxford University Press, New York, 1999).
[4] H. van Amerongen, L. Valkunas, and R. van Grondelle, *Photosyntetic Excitons* (World Scientific, Singapore, 2000).
[5] H. Zuber and R. A. Brunishplz, *Photosynthesis: Physical Mechanism and Chemical Patterns* (Cambridge University Press, New York, 1980).
[6] D. L. Andrews and A. A. Demidov, *Resonance Energy Transfer* (Wiley, New York, 1999).
[7] T. Kobayashi, *J-aggregates* (World Scientific, Singapore, 1996).
[8] R. H. Dicke, Phys. Rev. **93**, 99 (1954).
[9] S. Mukamel, Annu. Rev. Phys. Chem. **51**, 691 (2000).
[10] T. Meier, Y. Zhao, V. Chernyak, and S. Mukamel, J. Chem. Phys. **107**, 3876 (1997).
[11] J. Grad, G. Hernandez, and S. Mukamel, Phys. Rev. A **37**, 3835 (1988).
[12] S. De Boer and D. A. Wiersma, Chem. Phys. Lett. **165**, 45 (1990).
[13] F. C. Spano, J. R. Kuklinski, and S. Mukamel, Phys. Rev. Lett. **65**, 211 (1990).
[14] V. Chernyak, T. Meier, E. V. Tsiper, and S. Mukamel, J. Phys. Chem. A **103**, 10294 (1999).
[15] S. Weiss, Science **283**, 1676 (1999).

[16] X. S. Xie and J. K. Trautman, Annu. Rev. Phys. Chem. **49**, 441 (1998).
[17] H. Bach, A. Renn, G. Zumofen, and U. P. Wild, Phys. Rev. Lett. **82**, 2195 (1999).
[18] W. E. Moerner and L. Kador, Phys. Rev. Lett. **62**, 2535 (1989).
[19] M. Orrit and J. Bernard, Phys. Rev. Lett. **65**, 2716 (1990).
[20] I. S. Osad'ko, *Selective Spectroscopy of Single Molecules*, Springer Series in Chemical Physics Vol. 69, (Springer, Berlin, 2002).
[21] M. Lippitz, C. G. Hübner, T. Christ, H. Eichner, P. Bordat, A. Herrmann, K. Müllen, and T. Basché, Phys. Rev. Lett. **92**, 103001 (2004).
[22] Y. Zhao, T. Meier, W. M. Zhang, V. Chernyak, and S. Mukamel, J. Phys. Chem. B **103**, 3954 (1999).
[23] F. Kulzer and M. Orrit, Annu. Rev. Phys. Chem. **55**, 585 (2004).
[24] R. Verberk and M. Orrit, J. Chem. Phys. **119**, 2214 (2003).
[25] I. S. Osad'ko, JETP **82**, 434 (1996).
[26] D. Rutkauskas, V. Novoderezkhin, R. J. Cogdell, and R. van Grondelle, Biochemistry **43**, 4431 (2004).
[27] S. C. Kou, X. S. Xie, and J. S. Liu, Ann. Operat. Res. **54**, 469 (2005).
[28] I. S. Osad'ko and L. B. Yershova, J. Lumin. **87–89**, 184 (2000).
[29] H. J. Kimble, M. Dagenais, and L. Mandel, Phys. Rev. Lett. **39**, 691 (1977).
[30] L. Mandel, Opt. Lett. **4**, 205 (1979).
[31] R. Short and L. Mandel, Phys. Rev. Lett. **51**, 384 (1983).
[32] T. Basché, W. E. Moerner, M. Orrit, and H. Talon, Phys. Rev. Lett. **69**, 1516 (1992).
[33] S. C. Kitson, P. Jonsson, J. G. Rarity, and P. R. Tapster, Phys. Rev. A **58**, 620 (1998).
[34] C. G. Hübner, G. Zumofen, A. Renn, A. Herrmann, K. Müllen, and T. Basché, Phys. Rev. Lett. **91**, 093903 (2003).
[35] D. A. Bussian, M. A. Summers, B. Liu, G. C. Bazan, and S. K. Buratto, Chem. Phys. Lett. **388**, 181 (2004).
[36] M. Wu, P. M. Goodwin, W. P. Ambrose, and R. A. Keller, J. Phys. Chem. **100**, 17406 (1996).
[37] Ch. W. Hollars, S. M. Lane, and T. Huser, Chem. Phys. Lett. **370**, 393 (2003).
[38] P. Tinnefeld, K. D. Weston, T. Vosch, M. Cotlet, T. Weil, J. Hofkens, K. Müllen, F. C. De Schryver, and M. Sauer, J. Am. Chem. Soc. **124**, 14310 (2002).
[39] L. Valkunas, G. Trinkunas, and V. Liuolia, in *Resonance Energy Transfer* edited by D. L. Andrews and A. A. Demidov (Wiley, New York, 1999).
[40] L. Ying and X. S. Xie, J. Phys. Chem. B **102**, 10399 (1998).
[41] H. G. Dehmelt, Bull. Am. Phys. Soc. **20**, 60 (1975).
[42] R. Blatt and P. Zoller, Eur. J. Phys. **9**, 250 (1988).
[43] D. T. Pegg, R. Loudon, and P. L. Knight, Phys. Rev. A **33**, 4085 (1986).
[44] T. Basché, S. Kummer, and C. Bräuchle, Nature (London) **373**, 132 (1995).
[45] J. Bernard, L. Fleury, H. Talon, and M. Orrit, J. Chem. Phys. **98**, 850 (1993).
[46] M. S. Kim and P. L. Knight, Phys. Rev. A **36**, 5265 (1987).
[47] G. V. Varada and G. S. Agarwal, Phys. Rev. A **45**, 6721 (1992).
[48] A. Beige and G. C. Hegerfeldt, Phys. Rev. A **58**, 4133 (1998).
[49] C. Hettich, C. Schmitt, J. Zitzmann, S. Kühn, I. Gerhardt, and V. Sandoghar, Science **298**, 385 (2002).
[50] A. M. van Oijen, M. Ketelaars, J. Köhler, T. J. Aartsma, and J. Schmidt, Biophys. J. **78**, 1570 (2000).
[51] M. Ketelaars, A. M. van Oijen, M. Matsushita, J. Köhler, J. Schmidt, and T. J. Aartsma, Biophys. J. **80**, 1591 (2001).
[52] T. Vosch, J. Hofkens, M. Cotlet *et al.*, Angew. Chem., Int. Ed. **40**, 4643 (2001).
[53] H. P. Lu and X. S. Xie, Nature (London) **385**, 143 (1997).
[54] H. Yang, G. Luo, P. Karnchanaphanurach, T.-M. Louie, I. Rech, S. Cova, L. Xun, and X. S. Xie, Science **302**, 262 (2003).
[55] H. F. Arnoldus and G. Nienhuis, Opt. Acta **30**, 1573 (1983).
[56] I. S. Osad'ko and L. B. Yershova, J. Chem. Phys. **112**, 9645 (2000).
[57] Y. Zheng and F. L. H. Brown, J. Chem. Phys. **121**, 7914 (2004).
[58] P. W. Anderson, B. I. Halperin, and C. M. Varma, Philos. Mag. **25**, 1 (1971).
[59] R. Kubo, J. Math. Phys. **4**, 174 (1963).
[60] N. G. van Kampen, *Stochastic Processes in Physics and Chemistry* (North-Holland, Amsterodam, 1992).
[61] E. Geva and J. L. Skinner, J. Phys. Chem. B **101**, 8920 (1997).
[62] F. L. H. Brown and R. J. Silbey, J. Chem. Phys. **108**, 7434 (1998).
[63] A. M. Boiron, P. Tamarat, B. Lounis, R. Brown, and M. Orrit, Chem. Phys. **247**, 119 (1999).
[64] A. Zumbusch, L. Fleury, R. Brown, J. Bernard, and M. Orrit, Phys. Rev. Lett. **70**, 3584 (1993).
[65] E. Barkai, Y. Jung, and R. Silbey, Annu. Rev. Phys. Chem. **55**, 457 (2004).
[66] Y. Jung, E. Barkai, and R. Silbey, Adv. Chem. Phys. **123**, 199 (2002).
[67] S. Mukamel, *Principles of Nonlinear Optical Spectroscopy* (Oxford University Press, New York, 1995).
[68] Y. Zheng and F. L. H. Brown, J. Chem. Phys. **119**, 11814 (2003).
[69] R. J. Glauber, Phys. Rev. **131**, 2766 (1963).
[70] P. L. Kelley and W. H. Kleiner, Phys. Rev. **136**, A316 (1964).
[71] R. J. Glauber, in *Quantum Optics and Electronics*, edited by C. DeWitt, A. Blandin, and C. Cohen-Tannoudji (Gordon and Breach, New York, 1964).
[72] R. J. Cook, Phys. Rev. A **23**, 1243 (1981).
[73] D. Lenstra, Phys. Rev. A **26**, 3369 (1982).
[74] Y. He and E. Barkai, Phys. Rev. Lett. **93**, 068302 (2004).
[75] M. B. Plenio and P. L. Knight, Rev. Mod. Phys. **70**, 101 (1998).
[76] D. E. Makarov and H. Metiu, J. Chem. Phys. **115**, 5989 (2001).
[77] M. C. Wang and G. E. Uhlenbeck, Rev. Mod. Phys. **17**, 323 (1945).
[78] H. Risken,*The Fokker-Plank Equation* (Springer, Berlin, 1989).
[79] T. Jansen, W. Zhuang, and S. Mukamel, J. Chem. Phys. **121**, 10577 (2004).
[80] H. Tsunetsugu, T. Taniguchi, and E. Hanamura, Solid State Commun. **52**, 663 (1984).
[81] N. Wang, V. Chernyak, and S. Mukamel, J. Chem. Phys. **100**, 2465 (1994).
[82] V. Chernyak, N. Wang, and S. Mukamel, Phys. Rep. **263**, 213 (1995).
[83] G. S. Agarwal, *Springer Tracts in Modern Physics*, edited by G. Höhler (Springer, New York, 1974), Vol. 70.
[84] H.-P. Breuer and F. Petruccione, *The Theory of Open Quantum Systems* (Oxford University, New York, 2002).
[85] H. Glaeske, V. A. Malyshev, and K. H. Feller, Phys. Rev. A **65**, 033821 (2002).
[86] L. Mandel and E. Wolf, *Optical Coherence and Quantum Optics* (Cambridge University Press, New York, 1995).
[87] G. C. Hegerfeldt, Phys. Rev. A **47**, 449 (1993).
[88] A. G. Redfield, Adv. Magn. Reson. **1**, 1 (1965).
[89] S. Mukamel, Phys. Rev. A **68**, 063821 (2003).
[90] M. Merz and A. Schenzle, Appl. Phys. B: Photophys. Laser Chem. **50**, 115 (1990).
[91] K. S. Crump, J. Am. Chem. Soc. **23**, 89 (1976).
[92] J. T. Hsu and J. S. Dranoff, Comput. Chem. Eng. **11**, 101 (1987).
[93] E. Moreau, I. Robert, L. Manin, V. Thierry-Mieg, J. M. Gérard, and I. Abram, Phys. Rev. Lett. **87**, 183601 (2001).
[94] B. Fisher, J. M. Caruge, D. Zehnder, and M. Bawendi, Phys. Rev. Lett. **94**, 087403 (2005).
[95] F. Šanda and S. Mukamel, Phys. Rev. A **71**, 033807 (2005).
[96] G. H. Weiss, *Aspects and Applications of the Random Walks* (North-Holland, Amsterdam, 1994).
[97] A. I. Shushin, Phys. Rev. E **67**, 061107 (2003).
[98] F. Šanda and S. Mukamel, Phys. Rev. E **73**, 011103 (2006).